*Preprints* (www.preprints.org) | NOT PEER-REVIEWED | Posted: 4 July 2022 doi:10.20944/preprints202207.0026.v1

*Review*

# Hervé and Krebs Type Magnetic Polyoxometalate Dimers

Aleksandar Kondinski,[1,*] Abhishek Banerjee,[2,*] and Sib Sankar Mal[3,*]

[1] Department of Chemical Engineering and Biotechnology, University of Cambridge, Cambridge, UK
[2] Department of Chemistry, Visvesvaraya National Institute of Technology (VNIT), Nagpur – 440010, India
[3] Department of Chemistry, National Institute of Technology Karnataka (NITK), Surathkal, Mangalore - 575 025, Karnataka, India
* Correspondence: aleksandar@kondinski.com; abhishekbanerjee@chm.vnit.ac.in; malss@nitk.edu.in

**Abstract:** Lacunary polyoxometalates (POMs) are negatively charged metal–oxo clusters, formally obtained from plenary topologies via fragment removal. Owing to the fragment removal, the lacunary POMs archetypes are rich in nucleophilic terminal oxo ligands, making them suitable for post-synthetic coordination with various heterometals. Trilacunary heteropolytungstates (hetero-POTs) based on bowl-shaped $\{W_9O_{30}\}$ framework incorporating a central lone-pair containing $\{XO_3\}$ hetergroup (X = $As^{III}$, $Sb^{III}$, and $Bi^{III}$) function as all-inorganic scaffolds that in the presence of d-block metal cations typically construct sandwich-like dimers of Hervé and/or Krebs. Herein we review the preparative approaches, compositional and magnetic versatility of the constructing Hervé and Krebs type dimers and discuss prospective use as POMtronics.

**Keywords:** Polyoxometalates; dimers; polyoxotungstates; magnetism; synthesis; POMtronics

## 1. Introduction

The structural and chemical versatility of molecular assemblies allowing fine-tuning of the magneto chemical phenomena has been a driving force for the development of many magnetic chemicals at the nanoscale.[1] Magnetic molecules show the potential for quantum bit (i.e. "qubit") information storage as a superposition of states, which opens an emerging application in quantum computing.[2] Considering existing challenges such as loss of quantum coherence, practical deployment is currently out of reach;[3] however, at the same time, the field shows many encouraging prospects.[4]

Polyoxometalates (POMs) represent a class of molecular metal oxides, typically comprised of early transition metals in a high oxidation state (mainly V, Mo, and W).[5] POMs are one of the most complex of all-inorganic architectures,[6] with broad applications in catalysis,[7] materials science,[8] and nanoelectronics.[9] Owing to their all-inorganic nature, high symmetry and structural robustness, POMs have also been of high interest in molecular magnetism.[10] Plenary POMs exposing oxo-based cavities are typically used as scaffolds capable of stabilizing magnetic heterometallic cations, occasionally leading to single-ion magnets (SIMs) with spin qubit behaviour.[11] Prominent examples are the lanthanide functionalized Preyssler POMs,[10] and the cuboidal and pentagonal prismatic polyoxopalladates.[9a, 12] Some high symmetry, but partially or fully-reduced POMs, such as the semimetal-functionalized polyoxovanadates,[13] mixed-metal Keplerates[14] are known to exhibit complex magneto-chemical behaviour as well.[15] POMs with large internal cavities can exhibit multiple accessible oxo sites, successfully mimicking naturally occurring zeolites in incorporating multimetal magnetic nuclei,[16] or even full metal-oxo clusters.[17]

Low symmetry POMs deriving by formal removal of metal-oxo fragments from the plenary POM archetypes are another form of synthetic scaffolds that can function as inorganic polydentate ligands.[18] These types of POMs can coordinate to various 3d,[19] 4f,[20] or a combination of 3d/4f magnetically active metal centres.[21]

Preprints (www.preprints.org) | NOT PEER-REVIEWED | Posted: 4 July 2022 doi:10.20944/preprints202207.0026.v1



Owing to the good inertness of the W–O bonds, polytungstates (POTs) exhibit the most studied class of lacunary POMs.[22] Most of the lacunary POTs derive from the Keggin oidal archetype.[23] The kegginoidal archetype is often viewed as a clathrate, where most commonly, an $\{XO_4\}$ guest unit is encapsulated within an otherwise highly symmetrical and neutral $\{W_{12}O_{36}\}$.[23] These shelss' can be of $O_h$ or $D_{3h}$ symmetry, assigned respectively as $\alpha$- and $\beta$-Kegginoids (Figure 1). The formal removal of one $[WO]^{4+}$ unit leads to so-called monovacant or monolacunary POMs, which depending on the shell of derivation, can be further assigned as $\alpha$, and $\beta_{1\text{-}3}$.[24] The formal removal of two or more metal centres leads to a complex configuration isomer problem considering many possibilities where the formal removal can occur.[25] However, the trilacunary Kegginoids derived by a formal removal of the $\{W_3O_6\}$ moiety from the $\alpha$-/$\beta$-$\{W_{12}O_{36}\}$ are most studied. The formed $\{W_9O_{30}\}$ bowl-like ($C_{3v}$) metal oxo shells are inherently isomeric and can incorporate tetrahedral $\{XO_4\}$ or lone-pair containing trigonal pyramidal $\{XO_3\}$ units. In the case of $\{XO_4\}$, the guest unit can point with one terminal oxo towards the bottom of the bowl (configuration A) or towards the exterior (i.e. opening) of the $\{W_9O_{30}\}$ bowl (configuration B). Configuration B is commonly observed among lone pair containing $\{XO_3\}$ where X = $As^{III}$, $Sb^{III}$ and $Bi^{III}$. Other lone pair units such as $\{S^{IV}O_3\}$ or $\{Se^{IV}O_3\}$ have also been observed to be incorporated within the cavity; however, the formed POMs "dimerize" forming $[(XO_3)_2(WO_3)_{18}]^{n-}$ Wells-Dawson Type POMs.[24], [26]

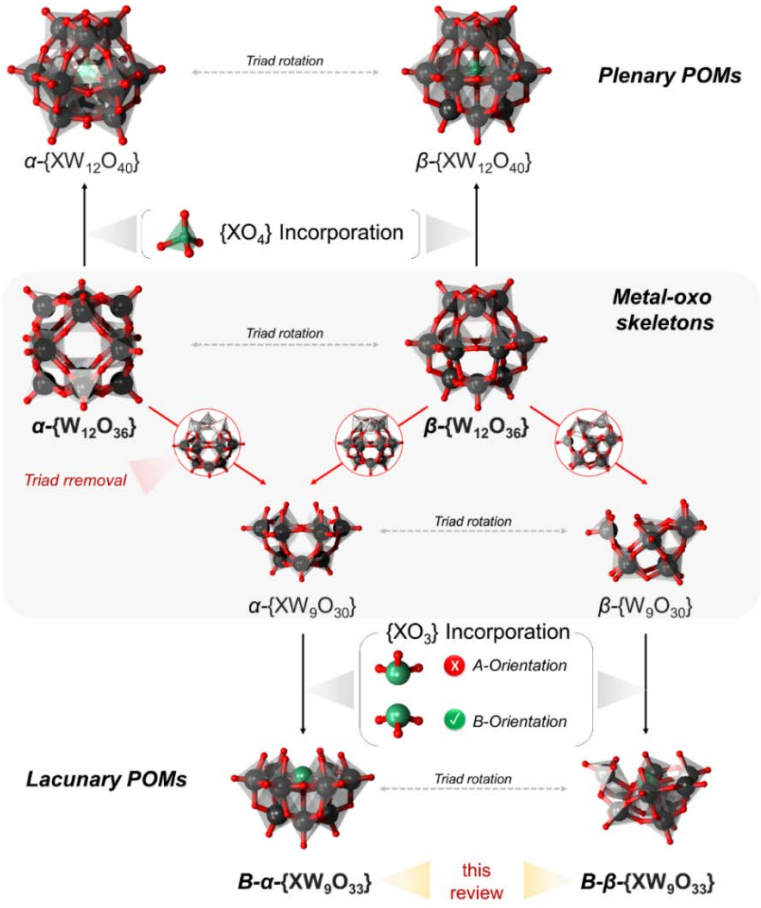


**Figure 1:** Schematic representation of the relationship between different metal–Oxo skeletons (middle row) and the incorporation of tetrahedral guests $\{XO_4\}$ leading to complete plenary POMs (top row) or $\{XO_3\}$ guests leading to different lone pair containing lacunary POMs (bottom row). Colour code: W = black, O = red.

The trilacunary $[XW_9O_{33}]^{9-}$ ligands readily form by the condensation reaction of acidified aqueous mixtures of $X_2O_3$ (X = $As^{III}$, $Sb^{III}$ and $Bi^{II}$.) and $Na_2WO_4{\cdot}2H_2O$, from an initial pH in the range between 7–9.[27] These POMs represent one of the most utilized lacunary

Preprints (www.preprints.org) | NOT PEER-REVIEWED | Posted: 4 July 2022 doi:10.20944/preprints202207.0026.v1



POMs for the preparation of heterometallic POMs. The lone pair and larger outward opening of these POMs makes them exhibit different reactivities, in contrast to the related $[XW_9O_{34}]^{n-}$ that adopt $\{XO_4\}$ units (X' = $P^V$, $Si^{IV}$, and $Ge^{IV}$).[28] This can be rationalized as the central O unit can also participate in binding,[29] typically leading to stabilization of tetrametallic fragments of layered double (hydro)oxide structure commonly referred to in the POM literature as the "Knoth dimer".[30] The lone pair is known to lead to so-called dimeric Knoth-type structures,[31] or via isomerization into Krebs-type dimeric structures,[27c] and many different open structures which can agglomerate several hundred or even thousands of atoms.[32]

This article focuses on sandwich-type complexes based on the tridentate B-type all-inorganic polyoxometalate ligands and the possibilities for their derivatization. In the first line, we review the electronic, structural, and reactivity properties of these lacunary POMs and discuss some general trends among them. Next, we systematically survey the incorporation of various heterometals, leading to a wealthy range of sandwich combinations and magnetic properties. We review the different structure topologies and the role of the lone pair sites and comment on their stability and magnetic properties.

## 2. Sandwich-type POM Archetypes

$\alpha$-$[XW_9O_{33}]^{9-}$ (X = $As^{III}$, $Sb^{III}$ and $Bi^{III}$) species exhibit six terminal oxo sites that are highly basic and able to coordinate to different hetero-metal centres. The oxo sites form a virtual distorted hexagonal plane normal to the 3–fold symmetric axis of rotation. The distortion can be traced to the arrangement of the central $\{XO_3\}$ unit, which shares its three oxo ligands with three pairs of tungsten centres, respectively. In this regard, the interatomic distances between terminal oxo centres that derive from a pair of edge-sharing $\{WO_6\}$ units (i.e. $d_a$(O···O)) differ from that between corner-sharing $\{WO_6\}$ units (i.e. $d_b$(O···O)). Standard geometry optimizations logically indicate that the relative difference between $d_a$(O···O) and $d_b$(O···O) is dependent on the nature of the X centres (Figure 2). The different X centres can lead to different charge distributions within $\alpha$-$[XW_9O_{33}]^{9-}$. The molecular electrostatic potentials reveal that the terminal oxo atoms in $\alpha$-$[AsW_9O_{33}]^{9-}$ are the most, while the relative basicity lowers gradually in $\alpha$-$[SbW_9O_{33}]^{9-}$ and then in $\alpha$-$[BiW_9O_{33}]^{9-}$.

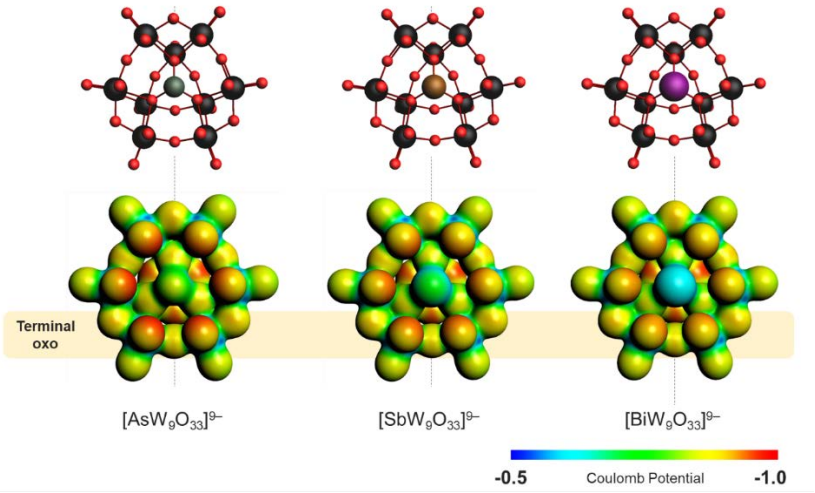


**Figure 2:** Ball-and-stick representation (top) and molecular electrostatic potential plotted over the density isosurface (bottom) of the three different trilacunary polyanions. Colour code: As = green, Sb = brown, Bi = violet, W = black and O = red. The most basic sites (bottom row) are shown with red colouring.

Another aspect of the reactivity of $\alpha$-$[XW_9O_{33}]^{9-}$ is how they connect and differ from other hetero-POTs comprised of the same building blocks. In order to discuss this aspect, we briefly focus on the chemistry of $\alpha$-$[AsW_9O_{33}]^{9-}$. In aqueous media $\alpha$-$[AsW_9O_{33}]^{9-}$ is

Preprints (www.preprints.org) | NOT PEER-REVIEWED | Posted: 4 July 2022 doi:10.20944/preprints202207.0026.v1



relatively reactive and can bind to additional mononuclear tungstate derivative building blocks. In the pH range between 3 – 4 and the presence of $Na^+$ cations, $\alpha$-$[AsW_9O_{33}]^{9-}$ interconnects with *cis*-$[WO_2]^{2+}$ bridging units, leading to tetrameric $[Na\subseteq(WO_2)_4(\alpha\text{-}AsW_9O_{33})_4]^{27-}$ polyanions.[33] On the other hand, when the *pH* reaches 6 and $K^+$ cations are present, $\alpha$-$[AsW_9O_{33}]^{9-}$ interconnects with *trans*-$[WO(H_2O)]^{4+}$ units leading to dimeric, sandwich-like $[K(H_2O)_n\{WO(H_2O)\}(\alpha\text{-}AsW_9O_{33})_2]^{13-}$ species (see section 3).[34] These structures show that pH and the nature of the cations have immense effect(s) upon the synthetic outcome, although to date, their exact role in the particular self-assembly process is not clear.[35]

Interaction of $\alpha$-$[XW_9O_{33}]^{9-}$ with heterometals (M) can lead to a wide range of structures differing in terms of POM ligands and interconnecting heterometal centres. As the trilacunary $\alpha$-$[XW_9O_{33}]^{9-}$ are polydentate ligands, their combination with high-coordinate cations (e.g., lanthanides or actinides) can result in many possible connectives and occasionally in oligomeric POMs assemblies with impressive tungsten nuclearities.[36] However, for improved synthetic and structural control, trilacunary $\alpha$-$[XW_9O_{33}]^{9-}$ have often been reacted with transition metal cations that have more modest coordination numbers, ultimately leading to a lower number of connecting possibilities.

If the metal cations are partially protected with non-labile ligands, they typically coordinate and saturate the lacunary site of $\alpha$-$[XW_9O_{33}]^{9-}$ POM, leading to metal-functionalized Janus-like nanomolecules. However, many transition metal cations deriving from simple metal salt precursors (e.g., chlorides, nitrates, etc.) can offer up to four coordination sites in square planar orientation and thus can interconnect two $\alpha$-$[XW_9O_{33}]^{9-}$ units in an archetype that due to historical reasons is referred to as Hervé-type POM sandwich.[37] For a more profound discussion here, we describe the Hervé-type sandwich as a liner POM assembly where a cationic $\{M_{6-x}\}$ belt (x = 0 - 5) is sandwiched between two $\alpha$-$[XW_9O_{33}]^{9-}$ units. The $\{M_{6-x}\}$ belt connects to six formerly terminal−oxo ligands deriving from both $\alpha$-$[XW_9O_{33}]^{9-}$ units. The $\{M_{6-x}\}$ is thus a part of a larger cyclic $\{M_{6-x}O_{12}\}$ fragment in which when x = 0, all M-centred $\{MO_4\}$ square planes or square pyramids $\{MO_4L\}$ are in edge-sharing configuration with one another. In a scenario when the $\{M_{6-x}\}$ belt is fully saturated (i.e., x = 0), one formally distinguishes between two configurational isomers obtained because of the orientation of the $\{XO_3\}$ units. When both units $\{XO_3\}$ units are oriented in an eclipsed fashion, the edge-sharing $\{WO_6\}$ octahedra from both $\alpha$-$[XW_9O_{33}]^{9-}$ units are also eclipsed (i.e., *syn*). The eclipsing provides differences in interatomic $d_{(O\cdots O)}$ distances and enforces an ideal $D_{3h}$ symmetry point group. The *syn* orientation is thus dominant among inter-POM bridging with three metal centres. However, the remaining sites to a "saturated $M_6$" scenario can often be occupied by metal cations with different coordination or ligand environment (e.g., alkali $Na^+$ and $K^+$).

When the two $\{XO_3\}$ units are in staggered (i.e., *anti*-) orientation, the remaining edge-sharing $\{WO_6\}$ octahedra are also staggered, and this enforces the lacunary sites to conform to a more "uniform" connectivity, which leads to an ideal $\{M_6O_{12}\}$ hexagonal belts. This is a profound difference and favours complete belt saturation. However, between the two very distinct sandwich archetypes $\{M_3(\alpha\text{-}XW_9O_{33})_2\}$ $D_{3h}$ and $\{M_6(\alpha\text{-}XW_9O_{33})_2\}$ $D_{3d}$ there are obviously other scenarios where 2, 4, and 5 metal centres are being sandwiched between $\alpha$-$[XW_9O_{33}]^{9-}$. In many of these configurations, partial occupancy or coordination changes induced by auxiliary ligands or other factors play a role that leads to different configurations, although from what we have reviewed here, the *syn* orientation is far more common than the *anti*. In most of the structures discussed, the linear alignment enforces closer proximity of the M centres, which in the case of spin-polarized centres can lead to interesting magnetic interactions and behaviour.

Preprints (www.preprints.org) | NOT PEER-REVIEWED | Posted: 4 July 2022 doi:10.20944/preprints202207.0026.v1



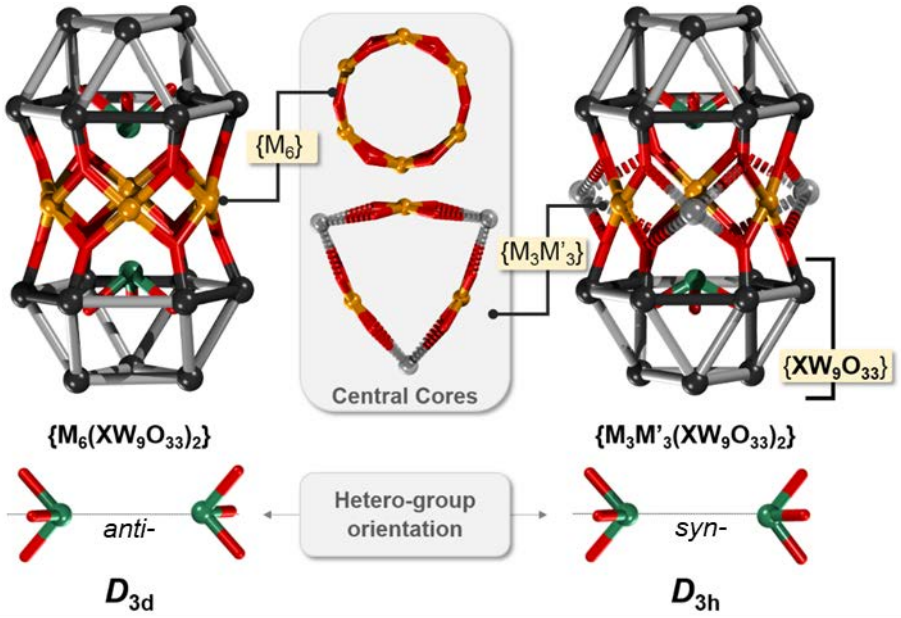


**Figure 3:** Ball and wireframe representation of the Linear/Hervé-sandwich $\{M_6(\alpha\text{-}XW_9O_{33})_2\}$ (left) and $\{M_3M'_3(\alpha\text{-}XW_9O_{33})_2\}$ archetype (right). The sandwiched $\{M_6\}$ and $\{M_3M'_3\}$ cores are shown in between, and the orientation of the two $\{XO_3\}$ units on the bottom. In the $\{XW_9O_{33}\}$ units, all oxo ligands except those participating in the sandwiching of the central belt cores have been omitted. Colour code: X = green, W = black and O = red. For grey and black wire, colouring is used to indicate corner and edge-sharing $\{WO_6\}$ octahedra.

The last profound change in the formation of complex assemblies is the isomerization of the $\alpha$-$[XW_9O_{33}]^{9-}$ to $\beta$-$[XW_9O_{33}]^{9-}$ (see Figure 1). While in the presence of transition metal cations, $\alpha$-$[XW_9O_{33}]^{9-}$ condensates in linear sandwich assemblies, the condensation of $\beta$-$[XW_9O_{33}]^{9-}$ favours an offset-sandwich assembly *vis-à-vis* $\{M_4O_{10}(XW_9O_{33})_2\}$, commonly referred to as the Krebs-type POMs.[27c, 38] The offset Krebs-type POM creates a belt of four centres forming a virtual rhomboid described by two geometrically inequivalent metal centres (a-site and b-site) placed along three different interatomic distances $d_1$ connecting a-b centres, $d_2$ connecting a-a centres, and $d_3$ connecting b-b centres as shown in Figure 4. The two most distant corners (i.e., those connected along $d_1$) are typically occupied by 3d centres, while the remaining directly bridging the $\beta$-$[XW_9O_{33}]^{9-}$ can be 3d transition metal or W-based. In the Krebs-type structures, the spin-polarized centres are often distant from one another and typically exhibit very weak or no magnetic coupling interactions.

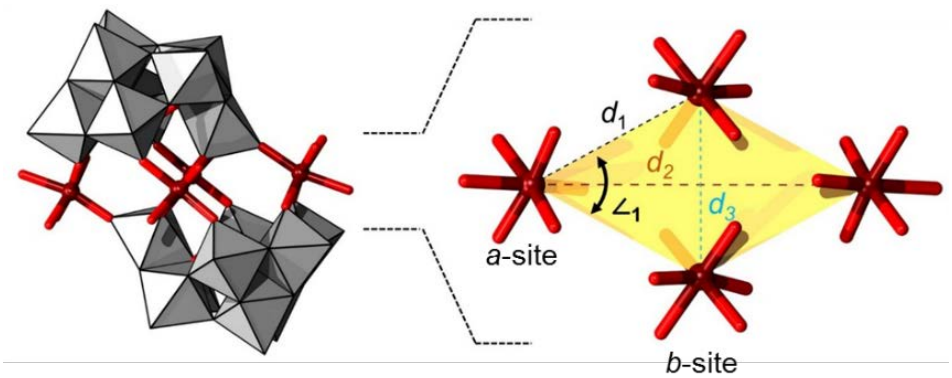


**Figure 4:** Offset/Krebs-type sandwich archetype $\{M_4O_{10}(\beta\text{-}XW_9O_{33})_2\}$ (left) and its central rhomboidal core (right) emphasizing the different *a*- and *b*-sites and $d_1$, $d_2$ and $d_3$ interatomic distances. Colour code: X = green (but covered), M = brown, $\{WO_6\}$ = grey octahedra, and O = red.

 doi:10.20944/preprints202207.0026.v1



## 3. Hervé type dimers

### 3.1. Atypical Hervé Polyanions

In 2001, Kortz and coworkers reported the sandwich type $[\{M^{II}_2(H_2O)_2\}\{WO\}(\alpha\text{-}AsW_9O_{33})_2]^{10-}$ where M = $Mn^{II}$, $Co^{II}$, $Zn^{II}$ (Figure 5.a).[39] In contrast to the classical Hervé-type POMs, this derived assembly incorporates only two heterometals, while a tungsten centre acts as another linking group between the two $\alpha$-$\{As^{III}W_9O_{39}\}$ units. Single crystal X-ray diffraction analysis revealed 79, 73, and 77% occupancy in the belt region for Mn, Co, and Zn, respectively. Elemental analysis revealed that, on average, two of the three belt positions of the dimeric polyanions are occupied by the first-row transition metal (Co, Mn, and Zn) and that the remaining position is occupied by a tungsten atom. The M–O bond distances for the polyanions range from 1.977 – 2.343, 1.95 – 2.284, and 1.967 – 2.227 Å for Mn, Co, and Zn, respectively.

An "open-sandwich" structure has been reported by Hussain and coworkers, *viz.* $[\{Ni(H_2O)_4\}_2\{WO(H_2O)\}(\alpha\text{-}AsW_9O_{33})_2]^{10-}$ (Figure 5.b).[40] In the latter polyanion. The latter structure is based upon the $\{(WO(H_2O))(\alpha\text{-}AsW_9O_{33})_2\}$ moiety, wherein two of the $\alpha$-$\{As^{III}W_9O_{39}\}$ units are joined at one corner with an octahedrally coordinated $\{WO_5(H_2O)\}$. The polyanion consists of two nickel atoms and one sodium atom coordinated to one of the $\alpha$-$\{As^{III}W_9O_{39}\}$ units.The sodium cation acts as a bridge between the two metal atoms. The other $\alpha$-$\{AsW_9O_{39}\}$ unit does not bond with nickel atoms but connects to the nickel coordinated $\alpha$-$\{AsW_9O_{39}\}$ Keggin unit via the $\{WO_5(H_2O)\}$ group, thus having a nominal $C_{2V}$ symmetry. The Ni–O distances in this polyanion range from 2.03 – 2.09 Å. Magnetic studies performed upon the polyanion using a vibrating-sample magnetometer show paramagnetic behaviour with the effective magnetic moment value calculated from data to be 3.23 B.M. (Bohr Magneton).

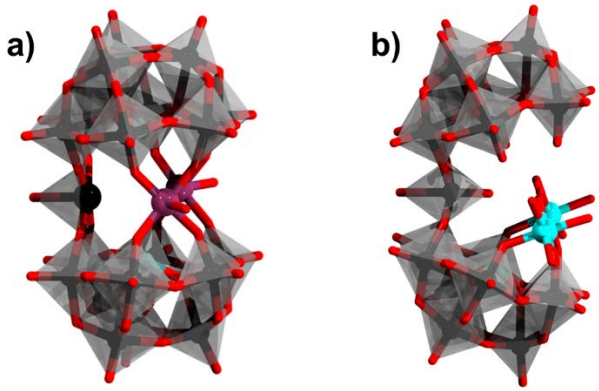


**Figure 5:** a) $[\{Co_2(H_2O)_2\}\{WO\}(\alpha\text{-}AsW_9O_{33})_2]^{10-}$; b) $[\{Ni(H_2O)_4\}_2\{WO(H_2O)\}(\alpha\text{-}AsW_9O_{33})_2]^{9-}$. Colour code: As = green, Co = purple, Ni = cyan, $\{WO_6\}$ = grey octahedra, W = black and O = red. Hydrogen atoms from aqua ligands are omitted.

### 3.2. Hervé Polyanions Sandwiching Three Heterometals

#### 3.2.1. Aqua terminating ligands

In 1982 Herve and coworkers reported the polyanion $[Cu_3(H_2O)_2(As^{III}W_9O_{39})_2]^{12-}$, consisting of a trimeric assembly of $Cu^{II}$ atoms, arranged in the pattern of an isosceles triangle (Cu···Cu distances = 4.669 and 4.707 Å), sandwiched between two $\alpha$-$\{AsW_9O_{39}\}$ units.[37] Interestingly, the two $\alpha$-$\{As^{III}W_9O_{39}\}$ subunits are not observed to face each other exactly. The three $Cu^{II}$ atoms are not equivalent in the polyanion, with two of the $Cu^{II}$ ions having a square planar geometry coordinated with oxygens from the polyanion units, while one

Preprints (www.preprints.org) | NOT PEER-REVIEWED | Posted: 4 July 2022 doi:10.20944/preprints202207.0026.v1



$Cu^{II}$ ion having a square pyramidal geometry with additional oxygen at the axial position. The Cu–O bond distances in this polyanion are in the range of 1.87 – 2.39 Å. The magnetic properties of this compound, reported in 1988, showed intramolecular anti-ferromagnetic coupling between the Cu atoms with $J$ = -7.5 K (~ -5.2 $cm^{-1}$).[41]

In 2001, the latter species were revisited when a group of $[(\alpha\text{-}XW_9O_{33})_2M_3(H_2O)_3]^{12-}$ where M = $Cu^{II}$, $Zn^{II}$; X = $As^{III}$, $Sb^{III}$ was reported.[39] The principal difference in the formation of $[(M(H_2O)_3)_3(\alpha\text{-}AsW_9O_{33})_2]^{12-}$ (pH range = 6.2 – 6.9) versus $[(M(OH_2))_2(WO(H_2O))(\alpha\text{-}AsW_9O_{33})_2]^{10-}$ (pH range = 3.9 – 4.8) is the pH maintained during synthesis. The Cu–O bond distances in this polyanion were also reported to be in the range of 1.87 – 2.39 Å. Analogous derivatives with $Se^{IV}$ and $Te^{IV}$ also with $Cu^{II}$, $[(Cu(OH_2))_3(\alpha\text{-}XW_9O_{33})_2]^{10-}$ (X = $Se^{IV}$, $Te^{IV}$) were also reported in the same article. The sandwich-type assembly in this polyanion joining the two $\alpha$-$[XW_9O_{33}]^{9-}$ units are also made of three isolated $Cu^{II}$ atoms. However, unlike the previously reported polyanions, in $[\{M(H_2O)_3\}_3(\alpha\text{-}AsW_9O_{33})_2]^{12-}$,[39] all the transition metals possess a square-pyramidal coordination geometry having four equatorial oxygens from the base polyanion units and one terminally coordinated water molecule at the axis; which now results in an idealized $D_{3h}$ symmetry for the title polyanions. The transition metals are now observed to be bridged with each other by sodium ions in the solid-state structure. Magnetic susceptibility data indicate a single anti-ferromagnetic spin-exchange constant $J$ for the triangular {$Cu_3$} belts with $J$ = -1.36 $cm^{-1}$ for $[(Cu(H_2O))_3(\alpha\text{-}AsW_9O_{33})_2]^{12-}$.[42]

The isostructural antimony derivative $[(Cu(OH_2))_3(\alpha\text{-}SbW_9O_{33})_2]^{12-}$ has been synthesized by reactions of $\alpha$-$[SbW_9O_{33}]^{9-}$ with $CuCl_2{\cdot}2H_2O$ or alternatively with $CuNO_3{\cdot}3H_2O$ in aqueous media under heating.[43] In the latter structure, the $Cu^{II}$ centres are in square planar coordination surrounded by four bridging oxo and a single terminal aqua ligand (Figure 6). As $Cu^{II}$ is a $d^9$ complex with one unpaired electron, magnetically this sandwich POM can be considered somewhat similar to $[(V^{IV}O)_3(\alpha\text{-}SbW_9O_{33})_2]^{12-}$ derivative. The anti-ferromagnetic coupling constant $J$ = 1.04$cm^{-1}$, while the ground state of the structure is S = ½. Magnetic hysteresis shows that the sandwich POM can be excited to the S = $^3/_2$ level.[42a, 44] By formal exchange of Sb centre with other p block elements, it has been shown that magnetisation can be minorly altered.[42a, 44] The $[(Cu(OH_2))_3(\alpha\text{-}SbW_9O_{33})_2]^{12-}$ has also been found to act as a modular component for the formation of hybrid inorganic–organic networks materials synthesized in the presence of alendronate ligands.[45]

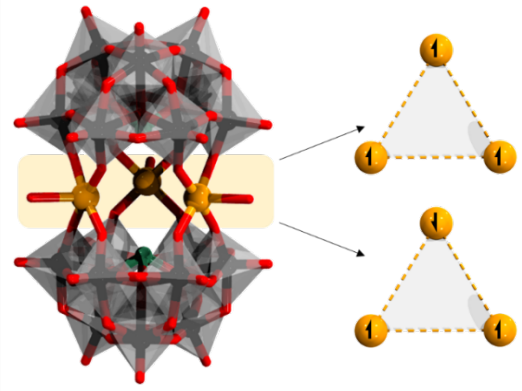

**Figure 6:** Representation of $[(Cu(OH_2))_3(\alpha\text{-}SbW_9O_{33})_2]^{12-}$ (left) and depiction of the spin orientation on the three $Cu^{II}$ sandwiched heterometals. Colour code: X = green (but covered), M = brown, {$WO_6$} = grey octahedra, W = black and O = red. Hydrogen atoms from aqua ligands are omitted.

In 2002, David and coworkers studied the bismuth derivatives and reported $[(Cu(OH_2))_3(\alpha\text{-}BiW_9O_{33})_2]^{12-}$ and $[(Mn(OH_2))_3(\alpha\text{-}BiW_9O_{33})_2]^{12-}$ derivatives,[46] which have been part of further investigations. The magnetic moment of $[(Cu(OH_2))_3(\alpha\text{-}BiW_9O_{33})_2]^{12-}$ was measured in the temperature range between 2 and 200 K. The spin-exchange factor $J$ = -7500 $cm^{-1}$ was observed with a Curie temperature $\theta_c$ = -1.58 K, consistent with g = 4.65.[47]

Preprints (www.preprints.org) | NOT PEER-REVIEWED | Posted: 4 July 2022 doi:10.20944/preprints202207.0026.v1



EPR measurements of $[(Cu^{II}(OH_2))_3(\alpha\text{-}BiW_9O_{33})_2]^{12-}$ revealed the anti-ferromagnetic coupling between the $Cu^{II}$ ions involve spin frustration, leading to a doubly degenerate S =1/2 ground states (EPR inactive) and an S = 3/2 excited state (EPR active).[48] In $[(Mn(OH_2))_3(\alpha\text{-}BiW_9O_{33})_2]^{12-}$ the Mn···Mn interatomic distances are in the range of 4.2 - 5.1 Å, which makes the dipolar interactions be smaller than the superexchange. The EPR spectra of $[(Mn(OH_2))_3(\alpha\text{-}BiW_9O_{33})_2]^{12-}$ revealed that each $Mn^{II}$ ion is antiferromagnetically coupled through either the $\alpha$-{$BiW_9O_{33}$} units or through space bipolar interactions. At the excited state of S =7/2, the isotopic exchange constant, estimated in the temperature range of 5–225 K, is $J$ = -2.074 $cm^{-1}$ and the zero-field splitting parameters D = -0.381 $cm^{-1}$, E = 0.054 $cm^{-1}$.[46]

### 3.2.2. Oxo terminating ligands

Similarly to $[(M(H_2O))_3(\alpha\text{-}AsW_9O_{33})_2]^{12-}$ (M = $Mn^{II}$, $Co^{II}$, $Ni^{II}$), Mialane and coworkers reported $[(VO)_3(\alpha\text{-}AsW_9O_{33})_2]^{11-}$, featuring three cationic {VO} moieties.[43b] Titration of the polyanion with $Ce^{IV}$ revealed that $[(VO)_3(\alpha\text{-}AsW_9O_{33})_2]^{11-}$ is a mixed-valent $\{V^{IV}_2V^{V}\}$ species. The terminal oxo atoms lead to shorter metal–oxygen bond lengths ca. 1.6 Å, in contrast when a terminal aqua ligand is bonded (ca. 2.0 Å). The vanadium derivative, however, showed significant disorder on two of the three metals linking the {$\alpha$-$AsW_9O_{33}$} units. For these two vanadium atoms, the V=O bonds are directed alternatively towards the inside or the outside of the sandwich interior (Figure 7). Magnetic studies on the polyanions reveal anti-ferromagnetic interactions between the metal centres with coupling constants $J$ = -2.9 $cm^{-1}$.

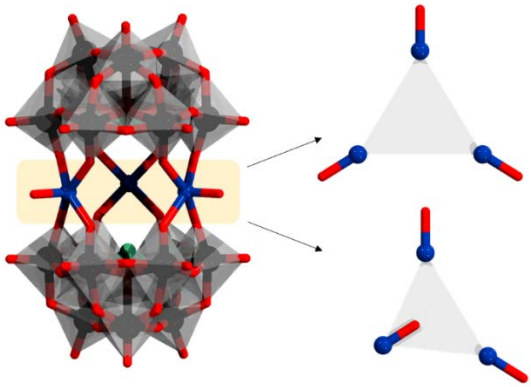

**Figure 7:** $[(V^{IV}O)_3(\alpha\text{-}AsW_9O_{33})_2]^{12-}$ (left) and the two different orientations of the cationic {VO}. Colour code: X = green (but covered), V = dark blue, {$WO_6$} = grey octahedra, W = black and O = red.

In 2001, Yamase reported the synthesis of the polyanion $[(V^{IV}O)_3(\alpha\text{-}SbW_9O_{33})_2]^{12-}$.[49] This POM was obtained from the reaction of $[\alpha\text{-}SbW_9O_{33}]^{9-}$ and $VOSO_4{\cdot}5H_2O$ in aqueous sodium acetate buffer at pH 4.8. In the later structures, the vanadium centres appear as {$VO_5$} square pyramids, and in such form, they normally can undergo reversible redox processes between vanadium(IV) and vanadium(V). Based on circular voltammetry, it was indeed shown that $[(V^{IV}O)_3(\alpha\text{-}SbW_9O_{33})_2]^{12-}$ can undergo three one-electron oxidations, that is, forming diamagnetic $[(V^{V}O)_3(\alpha\text{-}SbW_9O_{33})_2]^{12-}$ species. The circular voltammogram is quasi-reversible, which suggested that the POM retains its structural integrity in the solution. In the ground state, the sandwiched core of $[(V^{IV}O)_3(\alpha\text{-}SbW_9O_{33})_2]^{12-}$ is virtually identical to that reported for the arsenic analogue (Figure 7). In the $[(V^{IV}O)_3(\alpha\text{-}SbW_9O_{33})_2]^{12-}$ sandwich structures, the interatomic $V^{IV}$···$V^{IV}$ distances are 5.4–5.5 Å. Owing to the geometric frustration of the three centres, the particular POM shows a ground state is $S$ = 1/2. Based on magnetic hysteresis, it has been shown that magnetisation of the POM can cross from $S$ = 1/2 level to $S$ = 3/2. The later step is associated with a half step magnetisation, which normally is expected for an anti-ferromagnetic spin triangle.[50] The Yamase group also studied the spin frustrated $[(VO)_3(\alpha\text{-}BiW_9O_{33})_2]^{12-}$.[50-51] The authors observed an

Preprints (www.preprints.org) | NOT PEER-REVIEWED | Posted: 4 July 2022 doi:10.20944/preprints202207.0026.v1



unusual phenomenon of the magnetisation of $[(VO)_3(\alpha\text{-}BiW_9O_{33})_2]^{12-}$ jumps with distinct hysteresis for the S = ½ ↔ S =3/2 levels, crossing under fast sweeping pulsed magnetic field (~$10^3$ T/s) at the low temperature of 0.5 K and shorter pulse field. This hysteresis is expected for an anti-ferromagnetic spin triangle with anti-symmetrical Dzyaloshinky-Moriya interactions. The level-crossing field estimated zero-field splitting energies of 5−7 K between S =1/2 and S = 3/2 states for both polyanions for the magnetisation. Due to the three equivalent, I = 7/2 nuclei, and the hyperfine structures could be measured as well.

### 3.2.3. Other types of terminating ligands

When other N- or O-terminating organic ligands are present as part of the synthesis course, it is possible that these ligands will coordinate with the three sandwiched heterometals. The coordinating ligand may or may not lay in the same plane as the rest of the three heterometal centres showing a form of conformational isomerism.

Termination with pyridine (pyr, $C_5H_5N$) has been manifested in the preparation of $[(Ni(pyr))_3(\alpha\text{-}AsW_9O_{33})_2]^{12-}$ polyanions (Figure 8.a).[52] In the latter polyanions the terminal Ni−N bond is 2.016 Å, while the pyridine ligands lay in the same plane as the three heterometals. Magnetic susceptibility measurements have shown that the $Ni^{II}$ cations are not fully equivalent, leading to ferromagnetic Ni···Ni exchange as depicted by $J$ = 6.17 $cm^{-1}$. Similar to pyridine, functionalisation with aminopyrazine (apyr) also forms products through direct coordination as manifested in the polyanion $[(Ni(apyr))_3(\alpha\text{-}SbW_9O_{33})_2]^{12-}$.[53] In the latter antimonate derivative, the derived coupling constants $J_1$ = −0.39 $cm^{-1}$, $J_2$ = −1.07 $cm^{-1}$ are small and negative, indicating that the Ni···Ni exchange interactions are weak anti-ferromagnetic.[53]

Derivatives of 1,2,4-triazole (taz) have been reported for a number of polyanions $[(M(Htaz))_3(AsW_9O_{33})_2]^{9-}$ where M = $Mn^{II}$, $Co^{II}$, $Ni^{II}$ (Figure 8.b).[54] The latter polyanions show weak $M^{II}\cdots M^{II}$ ferromagnetic exchange interactions with $J_{Mn\cdots Mn}$ = - 0.36, $J_{Co\cdots Co}$ = 5.93, and $J_{Ni\cdots Ni}$ = 10.32.[54] Similarly, the binding of imidazole (imi) has been largely exploited, leading to anti-ferromagnetic systems of $[(M(imi))_3(\alpha\text{-}SbW_9O_{33})_2]^{12-}$ where M = $Mn^{II}$, $Ni^{II}$, $Co^{II}$, $Fe^{II}$, and $Cu^{II}$. The $Mn^{II}$, $Ni^{II}$ and $Co^{II}$ derivatives are obtained through the interaction of $Na_2WO_4{\cdot}2H_2O$ and $SbCl_3{\cdot}6H_2O$ (or alternatively $Sb_2O_3$) with the transition heterometal salt in the presence of imidazole.[55] The latter strategy does not work for creating copper derivatives,[56] and there the synthesis is based on the trilacunary $\alpha$-$[SbW_9O_{33}]^{9-}$.[57] The $Fe^{II}$ derivatives are also made using $\alpha$-$[SbW_9O_{33}]^{9-}$, but the iron comes as $Fe^0$ from iron powder in sodium acetate buffer.[58] Imidazole derivatives are also known based on the $\alpha$-$[BiW_9O_{33}]^{9-}$ unit. The polyanion $[(Co(imi))_3(\alpha\text{-}BiW_9O_{33})_2]^{12-}$ has been reported to appear as a product where copper based $\{Cu(imi)_4\}$ is grafted on the surface of the polyanion.[59] Magnetic susceptibility studies of $[(Co(imi))_3(\alpha\text{-}BiW_9O_{33})_2]^{12-}$ shows $J_{Co\cdots Co}$ = -19.2(4) $cm^{-1}$ assuming g = 2.005(2) and θ = -1.18(5) K, indicating anti-ferromagnetic behavior.

Use of 1-methylimidazole (mimi) has also led to the interesting derivatives, $[\{M(mimi)\}_3(\alpha\text{-}XW_9O_{33})_2]^{12-}$ where M = $Co^{II}$, $Mn^{II}$ and X = Sb and Bi.[60],[61] These derivatives show flexibility in the orientation of the imidazole ring in respect to the heteroatom plain (dihedral angle in the range of 13.7° to 89.7°). Magnetic susceptibility in the temperature range 2−300 K for $[(Co(mimi))_3(\alpha\text{-}BiW_9O_{33})_2]^{12-}$ showed $J$ = -0.053 $cm^{-1}$ and g = 2.02, whole for $[(Mn(mimi))_3(\alpha\text{-}BiW_9O_{33})_2]^{12-}$ $J$ = -0.06 $cm^{-1}$ and g = 1.99) have shown anti-ferromagnetic interaction. Coordination of outer acetate ligands has been recorded in $[(Mn(COOH))_3(\alpha\text{-}AsW_9O_{33})_2]^{15-}$ (Figure 8.c).[62] Magnetic susceptibility studies for these polyanions showed $J$ = 0.07 $cm^{-1}$ indicating a weak anti-ferromagnetic coupling between the $Mn^{II}$ centres.[62]

Preprints (www.preprints.org) | NOT PEER-REVIEWED | Posted: 4 July 2022 doi:10.20944/preprints202207.0026.v1



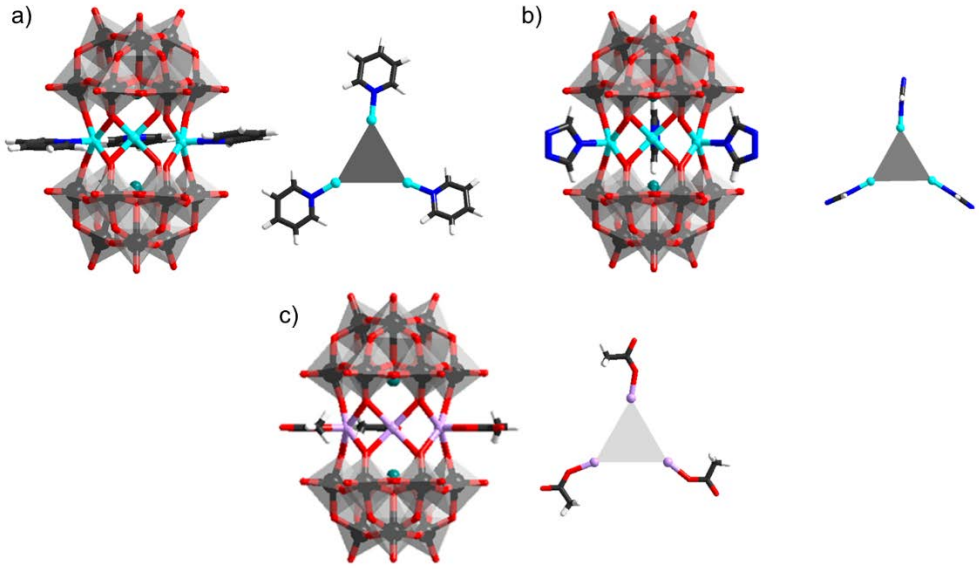


**Figure 8:** Polyanions and their heterometallic cores: a) $[(Ni(py))_3(AsW_9O_{33})_2]^{12-}$; b) $[(M(Htaz))_3(AsW_9O_{33})_2]^{9-}$; c) $[(Mn(COOH))_3(AsW_9O_{33})_2]^{15-}$. Colour code: As = green, Ni = cyan, Mn = light pink, H = white frame, C = dark grey frame, $\{WO_6\}$ = grey octahedra W = black and O = red.

### 3.3. Hervé Polyanions Sandwiching Two and Four Heterometals

Following the discussion on the *syn-* and *anti-* scenarios discussed in Figure 3 that apply for three and six heterometal sandwiching architectures, here we discuss the sandwiching of two and four heterometals. Considering a $D_{3d}$-symmetrized anti scenario, population with two centres will lead to 3 different configurational isomers (see Figure 9). On the other hand, using the same topology, population with four metal centres will similarly lead to 3 different isomeric configurations representing reversed populations. In case anti-isomerism is switched with *syn*-orientation, then distortion between the centres may occur.

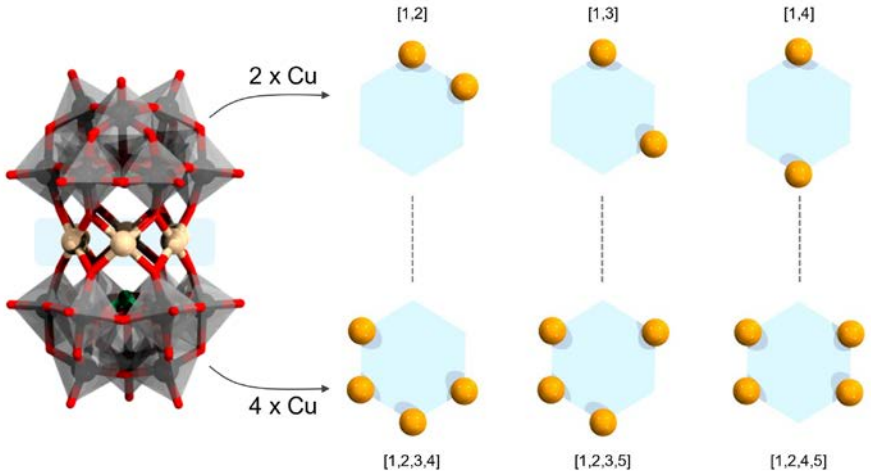


**Figure 9:** Generic sandwich $\{Cu_n(\alpha\text{-}XW_9O_{33})_2\}$ (left); isomers when n = 2 (top, right) and n = 4 (bottom, right). Colour code: X = green, Cu = (light) orange, $\{WO_6\}$ = grey octahedra, W = black and O = red.

The polyanion $[Cu_2(\alpha\text{-}SbW_9O_{33})_2]^{14-}$, obtained by the reaction of $Na_2WO_4{\cdot}2H_2O$, $Sb_2O_3$ and copper precursor in the presence of ethylenediamine, is an example of Hervé polyanion sandwiching two metal centres.[63] The involved ethylene diamine is not part of the Hervé motif, but a chelating agent to $Cu^{II}$ cations.[63] It is not clear to what extent by coor-

Preprints (www.preprints.org) | NOT PEER-REVIEWED | Posted: 4 July 2022 doi:10.20944/preprints202207.0026.v1



dinating to free $Cu^{II}$ ethylene diamine affects the active concentrations leading to two heterometal sandwiches. The resolved crystal structure of $[Cu_2Na_4(\alpha\text{-}SbW_9O_{33})_2]^{10-}$ indicates that sodium and copper cations are partially distributed around the six-metal belt, implying that the three isomer configurations may be possible. On the basis of magnetic susceptibility data for $[Cu_2(\alpha\text{-}SbW_9O_{33})_2]^{14-}$ it has been concluded that there are dominant ferromagnetic coupling interactions.[16]

The reversed heterometal populated sandwich $[Cu_4(\alpha\text{-}SbW_9O_{33})_2]^{10-}$ has been under hydrothermal conditions in the presence of diethylenetriamine.[64] Crystallographic study indicates that in the latter POM the scenario where pairs of $\{Cu_2O_6\}$ units sandwiched opposite to one another is prevanet (Is this word correct?).[64] Magnetic susceptibility data of $[Cu_4(\alpha\text{-}SbW_9O_{33})_2]^{10-}$ revealed weak anti-ferromagnetic coupling.[64]

Using $\alpha$-$\{As^{III}W_9O_{39}\}$ and $Cu^{II}$ atom, the polyanion $[Cu_4(H_2O)_4(\alpha\text{-}AsW_9O_{33})_2]^{10-}$ has also been reported.[65] The latter POM exhibits *syn*-like orientation where three copper oxo bridged cations are separated by two potassium cations from the remaining copper centres (Figure 10). Owing to the *syn* orientation, in comparison to the more idealized scenario (Figure 9.b), the heterometallic core of $[Cu_4(H_2O)_4(\alpha\text{-}AsW_9O_{33})_2]^{10-}$ appears slightly more distorted (Figure 10). However, the overall symmetry remains $C_{2v}$. The Cu−O bond lengths range from 1.91 – 2.31 Å within the $\{Cu_3O_8(H_2O)_9\}$ triad and from 1.95 – 2.55 Å within the isolated $\{CuO_4(H_2O)\}$ unit. Magnetic susceptibility data for the polyanion shows the presence of both ferromagnetically and antiferromagnetically coupled $Cu^{II}$ ions ($J_1$ = 2.78 ± 0.13 $cm^{-1}$, $J_2$ = -1.35 ± 0.02 $cm^{-1}$, and $J_3$ = -2.24 ± 0.06 $cm^{-1}$).

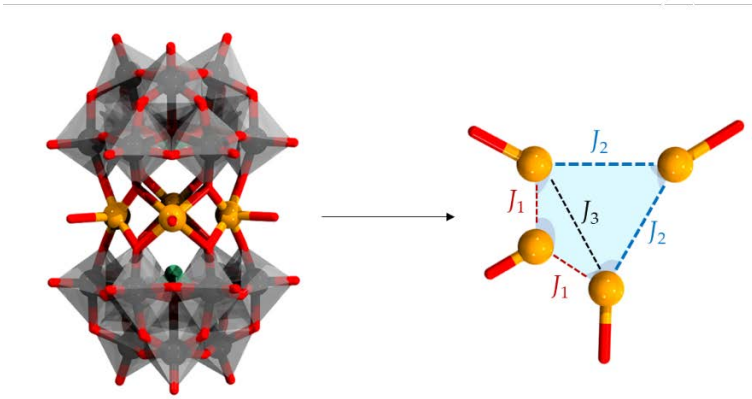


**Figure 10:** Polyanion $[Cu_4(H_2O)_4(\alpha\text{-}AsW_9O_{33})_2]^{10-}$ (left) and its $\{Cu\}_4$ core (right) depicting three different couplings ($J_1$, $J_2$ and $J_3$). Colour code: As = green, Cu = orange, $\{WO_6\}$ = grey octahedra, W = black and O = red.

### 3.4. Hervé Polyanions Sandwiching Five Heterometals

Furnishing the synthesis with bipyridine ligands can enforce symmetry break leading to structures with *syn* arrangement of the $\alpha$-$[SbW_9O_{33}]^{9-}$ units, which instead of three encapsulate five metal centres. Two polyanions of the type $[\{Mn(bpy)\}_2(MnCl)_3(AsW_9O_{33})_2]^{11-}$ and $[\{Mn(bpy)\}_2(MnCl)\{Mn(OH_2)\}_2(\alpha\text{-}SbW_9O_{33})_2]^{9-}$, where X = As and Sb and bpy is bipyridine, have been reported.[66] The manganese centres are connected to bipyridine, chloride, and aqua ligand (Figure 11.a). The Mn−N bond distance in the arsenic derivative is 2.25 Å, and the Mn−O bond distances are in the range of 2.08 – 2.24 Å. Magnetic studies on the polyanion show ferromagnetic interaction between the $Mn^{II}$ ions. On the other hand, imidazole can also lead to an unusual binding and formation of metal-carbon bonds between $Co^{II}$ and $Ni^{II}$, leading to $\{Na_{0.7}M_{5.3}(OH_2)_2(imi)_2(Himi)(\alpha\text{-}SbW_9O_{33})_2\}$ (Figure 11.b), that has partial sodium occupancy.[67]

Zhao and coworkers reported in 2013 a pentameric assembly of magnetically active metals with $\alpha$-$[AsW_9O_{33}]^{9-}$. The polyanion $[Na\subseteq Cu_5Cl(OH_2)_3(\alpha\text{-}AsW_9O_{33})_2]^{9-}$ has a hexagonal shaped $\{Cu_5Na\}$ assembly sandwiched between the two $\alpha$-$[AsW_9O_{33}]^{9-}$ units.[68] The metal ions in this sandwich, having identical square pyramidal geometry, are categorized

Preprints (www.preprints.org) | NOT PEER-REVIEWED | Posted: 4 July 2022 doi:10.20944/preprints202207.0026.v1



into four distinct groups based upon their coordination environment; viz. two identical {$CuO_4$}, one {$CuO_4(H_2O)$}, two disordered {$Cu/NaO_4(H_2O)$} and one {$CuO_4Cl$}. The Cu–O bond lengths in this polyanion range from 1.953 – 2.007 Å, while the Cu–Cl bond has a length of 2.5368 Å. Magnetic measurements for the polyanion revealed ferromagnetic exchange interactions within the {$Cu_5$} core mediated by the oxygen bridges.

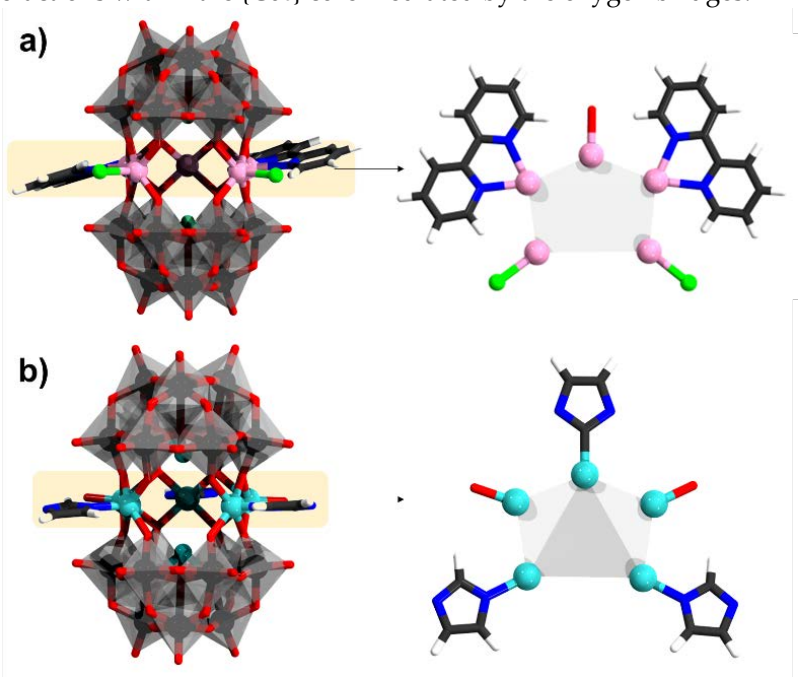


**Figure 11:** a) $[(Mn(bpy))_2(MnCl)(Mn(OH_2))_2(\alpha\text{-}SbW_9O_{33})_2]^{8-}$; b) $\{Na_{0.7}M_{5.3}(OH_2)_2(imi)_2(Himi)(\alpha\text{-}SbW_9O_{33})_2\}$. Colour code: X = green (but covered), M = brown, {$WO_6$} = grey octahedra W = black and O = red. The partial occupancy of $Na^+$ has been omitted.

### 3.5. Hervé Polyanions Sandwiching Six Heterometals

Saturated sandwich structures with six metal centres have been reported for $[(MnCl)_6(\alpha\text{-}XW_9O_{33})_2]^{12-}$ (Figure 12.a),[69] and $[(CuCl)_6(\alpha\text{-}XW_9O_{33})_2]^{12-}$.[70] These forms of sandwich structures are prepared using similar conditions as the trimetalate Hervé-type sandwiches, however, the synthesis is typically carried at ambient conditions, which may enhance slower sandwich closing giving time coordination between heterometals to occur. Both sandwich structures exhibit ferromagnetic coupling where for the ground state and the coupling constant for $[(CuCl)_6(\alpha\text{-}SbW_9O_{33})_2]^{12-}$ is $S$ = 3 ($J$ = +29.5 $cm^{-1}$) and $[(MnCl)_6(\alpha\text{-}SbW_9O_{33})_2]^{12-}$ is $S$ = 15 ($J$ = +0.14 $cm^{-1}$).[70-71] Further studies of the magnetic interactions for the polyanions $[(CuCl)_6(\alpha\text{-}AsW_9O_{33})_2]^{12-}$ and $[(MnCl)_6(\alpha\text{-}SbW_9O_{33})_2]^{12-}$ by Tsukerblat and coworkers gave coupling constants of $J$ = 35 and 0.55 $cm^{-1}$, respectively, and have also emphasized the importance of axial anisotropy towards explaining the magnetic properties of such arrangements.[72]

Linking of imidazole ligands produces $[M_6(imi)_6(\alpha\text{-}AsW_9O_{33}H_3)_2]$ where M = $Mn^{II}$, $Ni^{II}$, $Zn^{II}$ (Figure 12.b).[73] Magnetic susceptibility data for the nickel $J$ = +1.96 $cm^{-1}$ showing $Ni^{II}\cdots Ni^{II}$ ferromagnetic coupling. When instead of chloride ligands, oxalate ligands are involved, there is a possibility for the POM to grow further in the same plane with the hexametalate transition metal core. Using the oxalate addition, the ferromagnetic $[(Mn(ox))_3(Mn(H_2O)_3)_3(Mn(H_2O)_2)_2(Mn(H_2O))(\alpha\text{-}SbW_9O_{33})_2]^{6-}$ species have been isolated (Figure 12.c).[74]

Preprints (www.preprints.org) | NOT PEER-REVIEWED | Posted: 4 July 2022 doi:10.20944/preprints202207.0026.v1



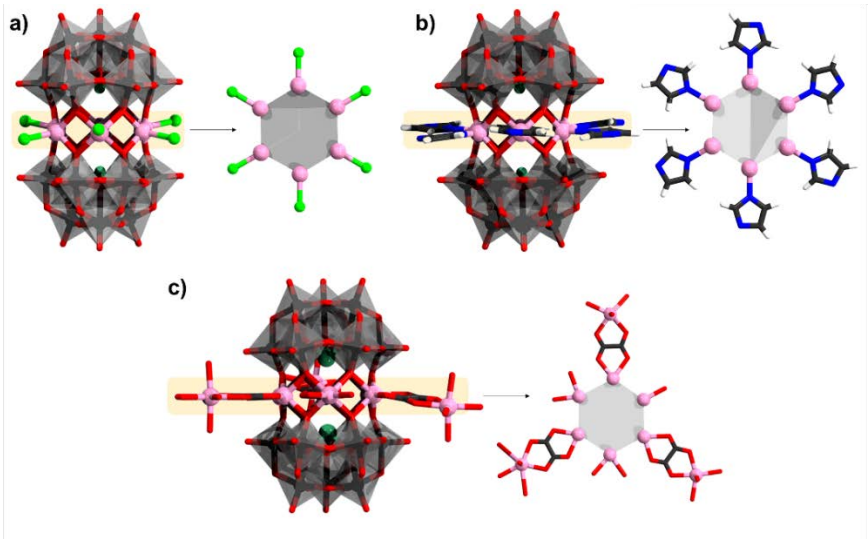


**Figure 12:** Polyanions and their heterometallic cores: a) $[(MnCl)_6(\alpha\text{-}SbW_9O_{33})_2]^{12-}$; b) $[Mn_6(imi)_6(\alpha\text{-}H_3AsW_9O_{33})_2]$; c) $[(Mn(ox))_3(Mn(H_2O)_3)_3(Mn(H_2O)_2)_2(Mn(H_2O))(\alpha\text{-}SbW_9O_{33})_2]^{6-}$. Colour code: As/Sb = green, Cl = light green, Mn = pink, N = blue, H = white, C = dark grey, {$WO_6$} = grey octahedra, W = black and O = red. H atoms on aqua ligands are omitted.

### 3.3. Hervé Polyanions Sandwiching Mixed-Metallic Cores

Besides the homometallic trimeric assemblies interspersed by alkali metal cations, several heterometallic assemblies with only transition metals and mixed transition metal-lanthanides have also been reported. One example is $[((V^{IV}O)_2Ln(H_2O)_4)(\alpha\text{-}AsW_9O_{33})_2]^{11-}$, where Ln = Dy and Gd (Figure 13.a).[75],[76] The polyanion shows an idealized $C_{2v}$ symmetry. V–O bond lengths ranging from ~1.6 – 1.99 Å and the Ln–O (Ln = Dy, Gd) bond lengths ranging from ~2.3 to 2.8 Å. The two $V^{IV}$ atoms in both the polyanions possess square pyramidal geometry with a short apical V=O bond of distance ~1.6 Å and are connected with each other via sodium counter cations. Ln centres in square antiprism coordination. Magnetic data for the polyanions showed weak anti-ferromagnetic interactions between the vanadium ($J_{VV}$ = -2.55 $cm^{-1}$) atoms and weak ferromagnetic interactions between vanadium and the lanthanide ($J_{GdV}$ = 0.6 $cm^{-1}$).

Another structure is $[M(OH_2)(Ti^{IV}O)_2(\alpha\text{-}As^{III}W_9O_{33})_2]^{12-}$ where M = $Co^{II}$, $Ni^{II}$, $Cu^{II}$ and $Zn^{II}$ (Figure 13.b).[77] The polyanion was synthesized by the reaction of the monovacant $[(Ti^{IV}O)_2(\alpha\text{-}As^{III}W_9O_{33})_2]^{14-}$,[78] with the respective metal. Magnetic studies on these polyanions indicate anti-ferromagnetic interactions with the nearest neighbours for these compounds, with effective magnetic moments calculated to be 5.45, 3.11, and 2.12 Bohr magnetons (B.M.) per molecule for M = $Co^{II}$, $Ni^{II}$, and $Cu^{II}$ respectively.

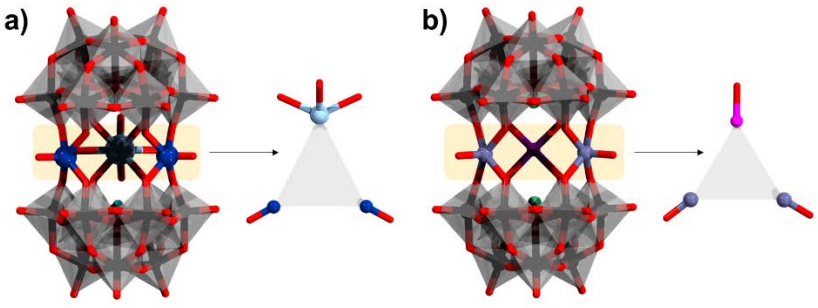


**Figure 13:** a) $[((V^{IV}O)_2Ln(H_2O)_4)(\alpha\text{-}AsW_9O_{33})_2]^{11-}$; b) $[Co(H_2O)(Ti^{IV}O)_2(\alpha\text{-}As^{III}W_9O_{33})_2]^{12-}$. Colour code: As = green, Ti = dark pink, Co = violet, V = dark blue, Gd = light blue, {$WO_6$} = grey octahedra, W = black and O = red. H atoms on aqua ligands are omitted.

Preprints (www.preprints.org) | NOT PEER-REVIEWED | Posted: 4 July 2022 doi:10.20944/preprints202207.0026.v1



Another is the polyanion $[Cu(H_2btp)Ln_{0.5}Na_{1.5}Cu_3(H_2O)_5(\alpha\text{-}AsW_9O_{33})_2]^{7-}$ where Ln = Ho, Yb, and btp is 1,3−bis[tris(hydroxymethyl)methylamino]propane (Figure 14).[79] The copper-organic group is in distorted octahedral geometry binding to two O and two N units. The moiety connects to the middle pentagonal metallocycle $\{Ln_{0.5}Na_{1.5}Cu_3(H_2O)_5\}$ cluster where one position is shared $[Ln_{0.5}/Na_{0.5}]^{2+}$ cation. The $[Ln_{0.5}/Na_{0.5}]^{2+}$ cation binds to eight oxygen atoms from the $\{\alpha\text{-}AsW_9O_{33}\}$ unit as well as two water ligands, achieving a square antiprism. The Ho/Na−O bond lengths range from 2.290 to 2.781 Å. Magnetic susceptibility data for the Ho derivative between 2 and 300 K was fitted according to the Curie-Weiss law, resulting in C = 11.21 emu K mol$^{-1}$ and θ = 2.89 K. The small positive $\theta$ value confirms the presence of the weak $Cu^{II}\cdots Ho^{III}$ ferromagnetic interactions.

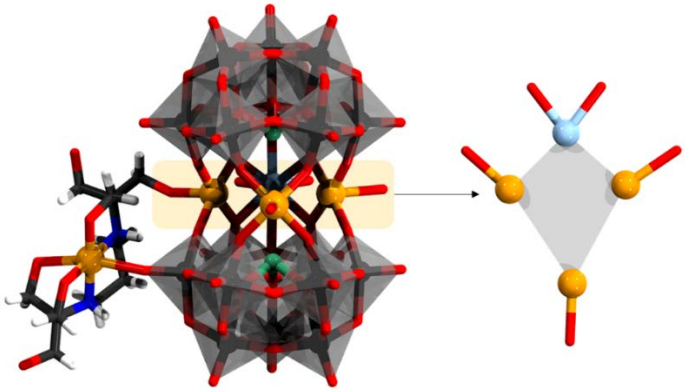

**Figure 14:** $[Cu(H_2btp)Ho_{0.5}Na_{1.5}Cu_3(H_2O)_5(\alpha\text{-}AsW_9O_{33})_2]^{11-}$ and its heterometallic core. Colour code: As = green, Cu = orange, N = blue, H = white, C = dark grey, Ho/Na = light blue, $\{WO_6\}$ = grey octahedra, W = black and O = red. H atoms on aqua ligands are omitted.

## 4. Krebs type dimers

### 4.1. Differentiation between classical Krebs dimers

Referring back to Figure 4, we generally distinguish between *a*- and *b*- site octahedra in the Krebs structure. As noted the interatomic distance between two a-sites (i.e., $d_2$) is ca. 10.0 Å, between two b-sites (i.e. $d_3$) it is ca. 5.6 Å, and between an a and b site (i.e., $d_1$) it is ca. ca. 5.4 Å. Overall, $d_1$, $d_2$, and $d_3$ are relatively large interatomic distances, and thus none or only very weak magnetic exchange interactions occur in this POM archetype.[80],[81]

The diamagnetic Krebs structure $[(WO_2OH)_2(WO_2)_2(\beta\text{-}SbW_9O_{33})]^{12-}$ is synthesized by reacting $\alpha\text{-}[SbW_9O_{33}]^{9-}$ with sodium tungstate in aqueous media. Early studies have shown that the structure can be post-functionalized with 3d metal cations (e.g., $Fe^{III}$, $Co^{II}$, $Mn^{II}$, $Ni^{II}$, and $Cu^{II}$).[27a],[81] The latter reactions lead to the formal substitution of the peripheral $\{WO_2OH\}$ units with $\{M(OH_2)_3)_2\}$ units, yielding $\{(M(OH_2)_3)_2(WO_2)_2(\beta\text{-}SbW_9O_{33})\}$ derivative species which can be doubly protonated.[27a],[81]

In addition to the typical synthetic pathways, mixtures of iron powder, imidazole, and pre-synthesized Krebs precursor $[(WO_2OH)_2(WO_2)_2(\beta\text{-}SbW_9O_{33})]^{12-}$ in acetic buffer solution under heating leads to the formation of the $Fe^{II}$ derivative $[Fe^{II}_2(H_2O)_6(WO_2)_2(\beta\text{-}SbW_9O_{33})_2]^{10-}$.[82] The latter structure is shown to be potential as catalyst for Fenton reaction and electrochemical sensing of ascorbic acid.[82]

The Krebs-like tetrametallic archetype $[M_4(H_2O)_{10}(\beta\text{-}SbW_9O_{33})_2]^{n-}$ has been reported for trivalent cations such as $Fe^{III}$, $Cr^{III}$, and $Al^{III}$ (Figure 15).[83] The $Fe^{III}$ and $Cr^{III}$ derivative has been obtained through a reaction of respective chloride salts with trilacunary precursors $\alpha\text{-}[XW_9O_{33}]^{9-}$ (X = As, Sb) in water at pH 3.0 under heating.[83a] Owing to the $Fe^{III}$ oxidation state, the polyanion $[Fe^{III}_4(H_2O)_{10}(\beta\text{-}SbW_9O_{33})_2]^{6-}$ is a subject to four electron reductions, which can lead to $[Fe^{II}_4(H_2O)_{10}(\beta\text{-}SbW_9O_{33})_2]^{10-}$ species. The latter interconversion is of relevance for catalytic oxygenation of catechol.[84] However, at the same time, it may be causing uncertainty in the accurate determination of the magnetic ground state of

Preprints (www.preprints.org) | NOT PEER-REVIEWED | Posted: 4 July 2022 doi:10.20944/preprints202207.0026.v1



$[Fe^{III}_4(H_2O)_{10}(\beta\text{-}SbW_9O_{33})_2]^{6-}$. Based on the isotropic Heisenberg Hamiltonian model, it was proposed that the ground state of the POM salt supposedly containing $[Fe^{III}_4(H_2O)_{10}(\beta\text{-}SbW_9O_{33})_2]^{6-}$ has a total spin of $S$ = 2,[85] however, X-ray photoelectron Fe 2p spectra have revealed that the iron centres $Fe^{II}$ formal valence state.[85] This deviation from the contained $Fe^{III}$ has been explained based on charge-transfer effects.[85]

Isolation of {Mn4}-Krebs derivative has been achieved with the help of manganese carbonyl cations $\{Mn(CO)_3\}$, leading to the polyanions $[\{Mn_4(H_2O)_{10}\}\{Mn(CO)_3\}_2(\beta\text{-}XW_9O_{33})_2]^{8-}$ (X = Sb and Bi).[86] Magnetic measurements of the latter compound at 1.8–300 K under a 2k Oe applied field suggest that the $Mn^{II}$ ions are strongly antiferromagnetically coupled.

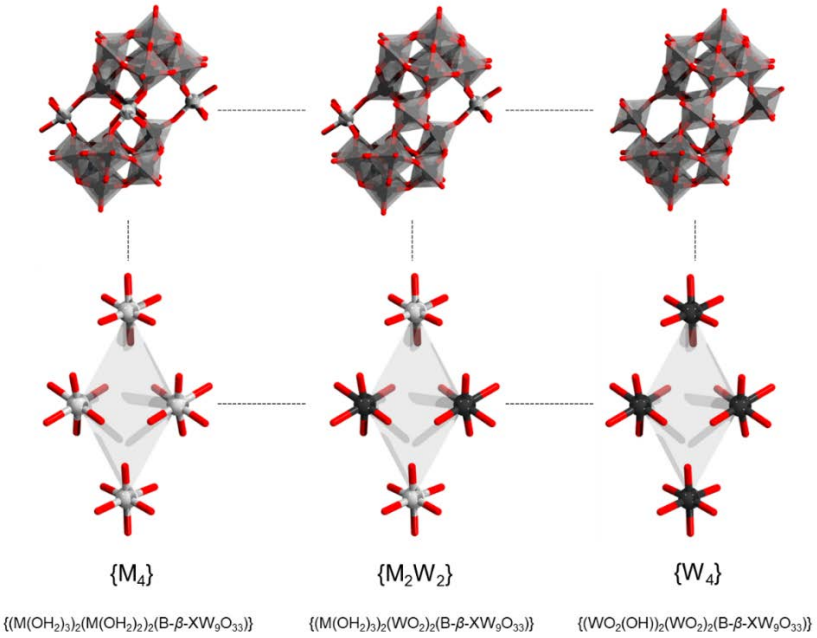


**Figure 15:** Offset/Krebs-type sandwich archetype (top row) and its sandwiched core (bottom) depicting full substitution with heterometals (left), partial substitution $\{M_2W_2\}$ (centre) and fully substitution with tungstate addenda $\{W_4\}$ units (right). Colour code: Sb = brown (but covered), M = grey, $\{MO_6\}/\{WO_6\}$ = grey octahedra W = black and O = red. H atoms on aqua ligands are omitted.

### 4.2. Partial substitutions in Krebs dimers

In the solid state, some Krebs-type polyanions may reflect compositions that deviate from the scenarios $\{(M(OH_2)_3)_2(WO_2)_2(\beta\text{-}SbW_9O_{33})\}$ and $\{M_4(H_2O)_{10}(\beta\text{-}XW_9O_{33})_2\}$ shown in Figure 15. However, currently, it is not clear if these partially substituted compositions reflect averages of $\{(M(OH_2)_3)_2(WO_2)_2(\beta\text{-}SbW_9O_{33})\}$ and $\{M_4(H_2O)_{10}(\beta\text{-}XW_9O_{33})_2\}$ in the crystallographic lattice, or individual POM entities with partial substitutions indeed are being formed. Examples of such polyanionic motifs in the solid state are: the discrete $[\{Mn_{3.5}W_{0.5}(H_2O)_{10}\}\{Mn(CO)_3\}_2(\beta\text{-}SbW_9O_{33})_2]^{4-}$,[86] $[Mn_{2.5}W_{1.5}(H_2O)_8(\beta\text{-}SbW_9O_{33})_2]^{4-}$,[87] and the chain-type $\{(Co(H_2O)_2)_3W(H_2O)_2(\beta\text{-}SbW_9O_{33})_2\}^{6-}$.[87] The latter two Mn-functionalized Krebs structures exhibit weak anti-ferromagnetic coupling ($\theta_c$ = -0.056 K in the range 50-300K).[87] A number of related species to $[(M(H_2O)_3)_2(M_{0.5}W_{0.5}O)_2(\beta\text{-}BiW_9O_{33})_2)]^{10-}$ where M = $Mn^{II}$, $Co^{II}$, $Ni^{II}$ have been produced in the presence of triethanolamine cations.[88]

### 4.3. Ligand substitution in Krebs dimers

Decorated Krebs structures can be prepared when the aqua ligands are linked to the heterometal M in $\{(M(OH_2)_3)_2(WO_2)_2(\beta\text{-}XW_9O_{33})\}$ and $\{M_4(H_2O)_{10}(\beta\text{-}XW_9O_{33})_2\}$ are exchanged. An example of such exchange is illustrated by $[Fe_2(DMSO)_8(WO)_2(\beta\text{-}XW_9O_{33})_2]^{4-}$ which has

Preprints (www.preprints.org) | NOT PEER-REVIEWED | Posted: 4 July 2022 doi:10.20944/preprints202207.0026.v1



been obtained by dissolving $[(Fe(OH_2)_3)_2(WO_2)_2(\beta\text{-}SbW_9O_{33})]^{8-}$ in DMSO, and recrystallizing it in the presence of ruthenium bipyridine cations.[89] Other strategy to exchange the aqua ligands maybe by introducing suitable binding ligands in the synthesis process. For instance, by introducing pyridine-3,4−dicarboxylate (pdc), the polyanion $[Fe_4(H_2O)_8(pdc)_2(\beta\text{-}SbW_9O_{33})_2]^{6-}$ (Figure 16.a) has been prepared instead of $[Fe^{III}_4(H_2O)_{10}(\beta\text{-}SbW_9O_{33})_2]^{6-}$.[90] Field-dependent magnetisation measurement for $[Fe_4(H_2O)_8(pdc)_2(\beta\text{-}SbW_9O_{33})_2]^{6-}$ at 2 K indicated $S = 7$ ground state.[90] The addition of oxalate (ox) can similarly lead to the formation of different products depending on the reaction pH. At pH = 3.0 discrete $[Fe^{II}_4(ox)_4(H_2O)_2(\beta\text{-}SbW_9O_{33})_2]^{14-}$ (Figure 16.b) polyanions are isolated,[80] while at pH = 6.0 chains of $\{Fe^{II}_4(ox)_4(\beta\text{-}SbW_9O_{33})_2\}_n$ are formed.[80] The presence of ethylenediamine during the formation process also leads of chain-like structures made of $\{Fe^{III}_4(H_2O)_8(\beta\text{-}SbW_9O_{33})_2\}$ components.[80]

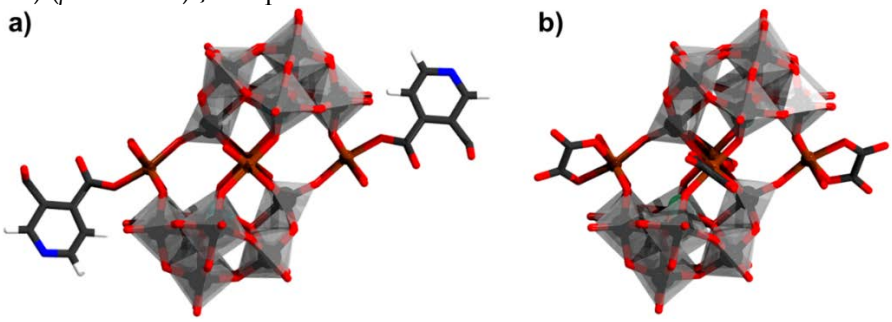


**Figure 16:** a) $[Fe_4(H_2O)_8(pdc)_2(\beta\text{-}SbW_9O_{33})_2]^{6-}$; b) $[Fe^{II}_4(ox)_4(H_2O)_2(\beta\text{-}SbW_9O_{33})_2]^{14-}$ Colour code: X = green (but covered), Fe = brown, $\{WO_6\}$ = grey octahedra, W = black and O = red. H atoms on aqua ligands are omitted.

If the added ligands are larger and have more than one binding site, then dimerisation maybe possible. By introducing N,O-chelating ligands such as pyrazine-2,3-dicarboxylate (pyzdc),[91] dimeric product $[(pyzdc)_2\{NaNi_2(H_2O)_4(WO_2)_2(\beta\text{-}SbW_9O_{33})_2\}_2]^{22-}$ containing two components of $[\{Ni(H_2O)_3\}_2(WO_2)_2(\beta\text{-}SbW_9O_{33})_2]^{10-}$ is obtained.[92] The dimerisation is also prevalent among Krebs-type polyanions with central belt involving heterometallic centres such as $Ni^{II}$, $Co^{II}$, or $Mn^{II}$),[93] as or Krebs type structures where the two tungstate metals at the a-sites are exchanged with tin heterogroups.[94]

### 4.4. Grafting metal cations and interconnecting Krebs dimers

The incorporation of transition metals and lanthanides within a single POM stabilized structure has been seen as a viable method for designing of 3d-4f complexes.[95] However, using the $[\alpha\text{-}SbW_9O_{33}]^{9-}$ polyanion incorporating both metal centres has been challenging. One reason is that the lanthanides have larger coordination spheres and often may lack directionality. In this regard, a number of structures containing Krebs-type complexes $[Fe^{II}_4(H_2O)_{10}(\beta\text{-}SbW_9O_{33})_2]^{10-}$ and lanthanide cations have been reported.[96] Such compounds have been obtained through the use of 2−picolinic acid (pic) leading to $[Fe^{II}_4(H_2O)_2(pic)_4(\beta\text{-}SbW_9O_{33})_2]^{10-}$ species and $[Ln(H_2O)_5]^{3+}$ cations where $Ln^{III}$ = $La^{III}$, $Pr^{III}$, $Nd^{III}$, $Sm^{III}$, $Eu^{III}$ (Figure 17.a).[96] Using a similar strategy and threonine (thr) ligands, another series of $[Fe^{III}_4(H_2O)_8(thr)_2(\beta\text{-}SbW_9O_{33})_2]^{6-}$ species interconnected with $[Ln(H_2O)_8]^{3+}$ cations where Ln = $Pr^{III}$, $Nd^{III}$, $Sm^{III}$, $Eu^{III}$, $Gd^{III}$, $Dy^{III}$, $Lu^{III}$ have been prepared.[97] Among the latter series, the $Eu^{III}$ derivatives have shown expected fluorescent emission.

Patzke and coworkers reported a series of 0-, 1-, 2-, and 3-dimensional copper-containing tungstobismuthate polyanions.[47] The reported complexes include the discrete $[Cu_2(H_2O)_4Cl_2(\beta\text{-}BiW_{10}O_{35})_2]^{12-}$ and $[Cu_2(H_2O)_6(\beta\text{-}BiW_{10}O_{35})_2]^{10-}$ polyanions. Two dimensional networks of $\{Cu_{0.5}Cl[Cu_2(H_2O)_4(\beta\text{-}BiW_{10}O_{35})_2]\}^{10-}$ (Figure 17.b), $\{Cu[Cu_2(H_2O)_4(\beta\text{-}BiW_{10}O_{35})_2]\}^{8-}$, $[Cu_3(H_2O)_3(\alpha\text{-}BiW_9O_{33})_2]^{12-}$ and three dimensional

Preprints (www.preprints.org) | NOT PEER-REVIEWED | Posted: 4 July 2022 doi:10.20944/preprints202207.0026.v1



$[(Cu_3Cl)(K_{2.62}Cu_{0.38}(H_2O)_3(\alpha\text{-}BiW_9O_{33})_2]^{9-}$ have also been reported. The copper centres in these series are relatively away from one another in the range of 8 to 11 Å.

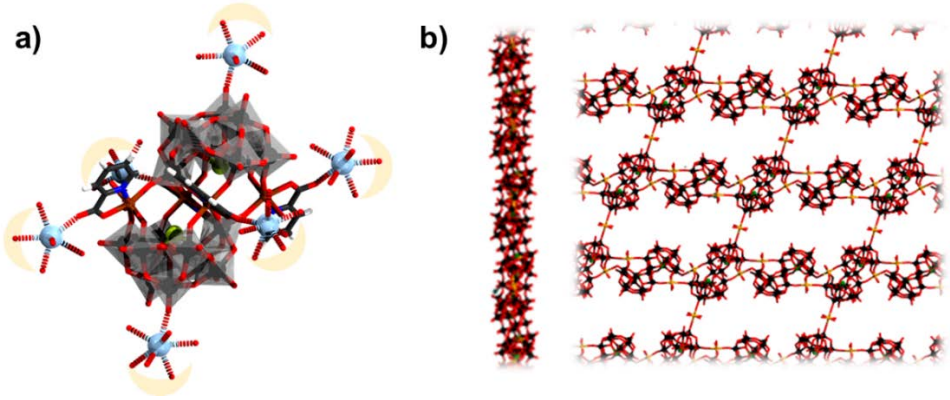


**Figure 17:** a) $La^{III}$ cations grafted on $[Fe^{II}_4(H_2O)_2(pic)_4(\beta\text{-}SbW_9O_{33})_2]^{10-}$; b) side and top view on two dimensional $\{Cu_{0.5}Cl[Cu_2(H_2O)_4(\beta\text{-}BiW_{10}O_{35})_2]\}^{10-}$. Colour code: X = green (but covered), La = light blue, Fe = brown, $\{WO_6\}$ = grey octahedra, W = black and O = red. H atoms on aqua ligands are omitted.

## 5. Conclusions

This article provided a comprehensive overview of the two most common sandwich-type archetypes in POM chemistry – Hervé and Krebs-type. The Hervé-type POMs generally adopt two main arrangements of the lavunary units and are capable to incorporate between two and six magnetic heterometals. The close arrangement of the metal centres typically causes spin interactions that leading to ferromagnetic and antiferromagnetic scenarios. The relative arrangement of the lacunary units also plays role in the number of incorporated centres. Considering the synthetic conditions, these types of POM dimers can be further functionalised with a variety of binding ligand and grafting cations. The Krebs-type polyanions appear to be more common for Sb- and Bi-based lacunary heteroPOMs. In the latter polyanion, the metal centres lay further apart from one another, and thus most of the interactions between magnetic heterocentres remain weakly antiferromagnetic. Both sorts of polyanions show stability to multielectron reductions, which is not only interesting in magnetism but in catalysis as well.

The present review provided first comprehensive structuring of magnetic POM sandwich dimes, which will be extended to other POM systems in future. Although currently it may be challenging to derive rules in which one can rationally design new sandwich POMs with desired magnetic properties, current applications of knowledge engineering[98] show promise such endavour to be achived in near future. In this regard, we also envision that magnetic POM dimers, would be of high interest in the development of future POM-based nanoelectronics (i.e. POMtronics).[99]

## Abbreviations

**apyr**: aminopyrazine

**bpy**: bipyridine

**btp**: 1,3–bis[tris(hydroxymethyl)methylamino]propane

**DMSO**: dimethyl sulfoxide

**imi**: imidazole

**mimi**: 1-methylimidazole

**ox**: oxalate

**pdc**: pyridine-3,4–dicarboxylate

**pyzdc**: pyrazine-2,3-dicarboxylate

 doi:10.20944/preprints202207.0026.v1



**pic**: 2−picolinic acid

**pyr**: pyridine

**taz**: 1,2,4−1H-triazole

**thr**: threonine

**Author Contributions:** Conceptualization, writing, review, and editing A.K., A.B., and S.S.M. All authors have read and agreed to the published version of the manuscript.

**Funding:** AK thanks Alexander von Humboldt Foundation and the Isaac Newton Trust for Post-doctoral fellowships.

**Conflicts of Interest:** The authors declare no conflict of interest.

## References

[1] A. Gaita-Arino, H. Prima-Garcia, S. Cardona-Serra, L. Escalera-Moreno, L. E. Rosaleny and J. J. Baldovi, *Inorg. Chem. Front.* **2016**, *3*, 568-577.

[2] a) S. Bertaina, S. Gambarelli, T. Mitra, B. Tsukerblat, A. Muller and B. Barbara, *Nature* **2008**, *453*, 203-U205; b) S. Hill, R. S. Edwards, N. Aliaga-Alcalde and G. Christou, *Science* **2003**, *302*, 1015-1018; c) V. Cerletti, W. A. Coish, O. Gywat and D. Loss, *Nanotechnology* **2005**, *16*, R27-R49; d) M. Atzori, E. Morra, L. Tesi, A. Albino, M. Chiesa, L. Sorace and R. Sessoli, *J. Am. Chem. Soc.* **2016**, *138*, 11234-11244; e) J. J. Baldovi, S. Cardona-Serra, J. M. Clemente-Juan, E. Coronado, A. Gaita-Arino and A. Palii, *Inorg. Chem.* **2012**, *51*, 12565-12574; f) P. C. E. Stamp and A. Gaita-Ariño, *J. Mater. Chem.* **2009**, *19*, 1718-1730.

[3] W. P. Schleich, *Nature* **2000**, *403*, 256-257.

[4] a) L. Escalera-Moreno, J. J. Baldovi, A. Gaita-Arino and E. Coronado, *Chem. Sci.* **2018**, *9*, 3265-3275; b) F. Donati, S. Rusponi, S. Stepanow, C. Wäckerlin, A. Singha, L. Persichetti, R. Baltic, K. Diller, F. Patthey, E. Fernandes, J. Dreiser, Ž. Šljivančanin, K. Kummer, C. Nistor, P. Gambardella and H. Brune, *Science* **2016**, *352*, 318; c) J. M. Zadrozny, J. Niklas, O. G. Poluektov and D. E. Freedman, *ACS Cent. Sci.* **2015**, *1*, 488-492; d) C. A. P. Goodwin, F. Ortu, D. Reta, N. F. Chilton and D. P. Mills, *Nature* **2017**, *548*, 439-442; e) K. Bader, D. Dengler, S. Lenz, B. Endeward, S. D. Jiang, P. Neugebauer and J. van Slageren, *Nat. Commun.* **2014**, *5*, 5304; f) F. S. Guo, B. M. Day, Y. C. Chen, M. L. Tong, A. Mansikkamaki and R. A. Layfield, *Angew. Chem. Int. Ed.* **2017**, *56*, 11445-11449.

[5] a) M. T. Pope and A. Müller, *Angew. Chem. Int. Ed.* **1991**, *30*, 34-48; b) D. L. Long, R. Tsunashima and L. Cronin, *Angew. Chem. Int. Ed.* **2010**, *49*, 1736-1758.

[6] S. V. Krivovichev, *Angew. Chem. Int. Ed.* **2014**, *53*, 654-661.

[7] S. S. Wang and G. Y. Yang, *Chem. Rev.* **2015**, *115*, 4893-4962.

[8] a) Y. F. Song and R. Tsunashima, *Chem. Soc. Rev.* **2012**, *41*, 7384-7402; b) Y. Ji, L. Huang, J. Hu, C. Streb and Y.-F. Song, *Energ. Environ. Sci.* **2015**, *8*, 776-789.

[9] a) J. J. Baldoví, L. E. Rosaleny, V. Ramachandran, J. Christian, N. S. Dalal, J. M. Clemente-Juan, P. Yang, U. Kortz, A. Gaita-Ariño and E. Coronado, *Inorg. Chem. Front.* **2015**, *2*, 893-897; b) X. Chen, Y. Zhou, V. A. L. Roy and S. T. Han, *Adv. Mater.* **2018**, *30*.

[10] J. M. Clemente-Juan, E. Coronado and A. Gaita-Arino, *Chem. Soc. Rev.* **2012**, *41*, 7464-7478.

[11] a) J. J. Baldovi, S. Cardona-Serra, J. M. Clemente-Juan, E. Coronado, A. Gaita-Arino and H. Prima-Garcia, *Chem. Commun.* **2013**, *49*, 8922-8924; b) M. Shiddiq, D. Komijani, Y. Duan, A. Gaita-Arino, E. Coronado and S. Hill, *Nature* **2016**, *531*, 348-351.

[12] J. J. Baldoví and A. Kondinski, *Inorganics* **2018**, *6*.

[13] K. Y. Monakhov, W. Bensch and P. Kogerler, *Chem. Soc. Rev.* **2015**, *44*, 8443-8483.

[14] P. Kogerler, B. Tsukerblat and A. Muller, *Dalton Trans.* **2010**, 21-36.

[15] K. Y. Monakhov, M. Moors and P. Kögerler in *Chapter Nine - Perspectives for Polyoxometalates in Single-Molecule Electronics and Spintronics*, *Vol. 69* Eds.: R. van Eldik and L. Cronin), Academic Press, **2017**, pp. 251-286.
[16] U. Kortz, A. Müller, J. van Slageren, J. Schnack, N. S. Dalal and M. Dressel, *Coord. Chem. Rev.* **2009**, *253*, 2315-2327.
[17] a) A. Kondinski and K. Y. Monakhov, *Chemistry - A European Journal* **2017**, *23*, 7841-7852; b) S. S. Mal and U. Kortz, *Angew. Chem. Int. Ed.* **2005**, *44*, 3777-3780.
[18] a) L. Shi, B. Li and L. X. Wu, *Chem. Commun.* **2015**, *51*, 172-175; b) C. Ritchie and C. Boskovic in *Polyoxometalates as Ligands for Functional Lanthanoid Complexes*, *Vol. Volume 8* World Scientific, **2013**, pp. 201-241.
[19] N. V. Izarova and P. Kögerler in *Chapter 06 - Polyoxometalates-based single molecule magnets*, Eds.: L. Ruhlmann and D. Schaming), Nova Science Publishers, **2015**, pp. 121-149.
[20] C. Boskovic, *Acc. Chem. Res.* **2017**, *50*, 2205-2214.
[21] S. Reinoso, *Dalton Trans.* **2011**, *40*, 6610-6615.
[22] W. G. Klemperer, *Inorg. Synth.* **1990**, 71-85.
[23] A. Kondinski and T. N. Parac-Vogt, *Front. Chem.* **2018**, *6*.
[24] H. Chermette and F. Lefebvre, *Cr. Chim.* **2012**, *15*, 143-151.
[25] C. Simms, A. Kondinski and T. N. Parac-Vogt, *(submitted)* **2020**.
[26] C. Busche, L. Vila-Nadal, J. Yan, H. N. Miras, D. L. Long, V. P. Georgiev, A. Asenov, R. H. Pedersen, N. Gadegaard, M. M. Mirza, D. J. Paul, J. M. Poblet and L. Cronin, *Nature* **2014**, *515*, 545-549.
[27] a) M. Bösing, I. Loose, H. Pohlmann and B. Krebs, *Chem. Eur. J.* **1997**, *3*, 1232-1237; b) K. C. Kim, A. Gaunt and M. T. Pope, *J. Cluster Sci.* **2002**, *13*, 423-436; c) I. Loose, E. Droste, M. Bösing, H. Pohlmann, M. H. Dickman, C. Rosu, M. T. Pope and B. Krebs, *Inorg. Chem.* **1999**, *38*, 2688-2694.
[28] M. T. Pope, X. Wei, K. Wassermann and M. H. Dickman, *Compt. Rend. Acad. Sci. Ser. C - Chemistry* **1998**, *1*, 297-304.
[29] A. Dolbecq, E. Dumas, C. R. Mayer and P. Mialane, *Chem. Rev.* **2010**, *110*, 6009-6048.
[30] T. J. R. Weakley, *J. Chem. Soc., Dalton Trans.* **1973**, 341-346.
[31] W. H. Knoth, P. J. Domaille and R. D. Farlee, *Organometallics* **1985**, *4*, 62-68.
[32] F. Hussain and G. R. Patzke, *CrystEngComm* **2011**, *13*, 530-536.
[33] F. Robert, M. Leyrie, G. Herve, A. Teze and Y. Jeannin, *Inorg. Chem.* **1980**, *19*, 1746-1752.
[34] U. Kortz, M. G. Savelieff, B. S. Bassil and M. H. Dickman, *Angew. Chem. Int. Ed.* **2001**, *40*, 3384-+.
[35] G. Hervé, A. Tézé and R. Contant in *General Principles of The Synthesis of Polyoxometalates in Aqueous Solution*, Eds.: J. J. Borrás-Almenar, E. Coronado, A. Müller and M. Pope), Springer Netherlands, Dordrecht, **2003**, pp. 33-54.
[36] F. Hussain, F. Conrad and G. R. Patzke, *Angew. Chem. Int. Ed.* **2009**, *48*, 9088-9091.
[37] F. Robert, M. Leyrie and G. Herve, *Acta Cryst. B* **1982**, *38*, 358-362.
[38] M. Sun, F. Li, L. Yu, Y. Wang and L. Xu, *Dalton Trans.* **2016**, *45*, 2417-2421.
[39] U. Kortz, N. K. Al-Kassem, M. G. Savelieff, N. A. Al Kadi and M. Sadakane, *Inorg. Chem.* **2001**, *40*, 4742-4749.
[40] M. K. Saini, R. Gupta, S. Singh and F. Hussain, *RSC Adv.* **2015**, *5*, 25273-25278.
[41] G. F. Kokoszka, F. Padula, A. S. Goldstein, E. L. Venturini, L. Azevedo and A. R. Siedle, *Inorg. Chem.* **1988**, *27*, 59-62.
[42] a) Ashley C. Stowe, S. Nellutla, Naresh S. Dalal and U. Kortz, *Eur. J. Inorg. Chem.* **2004**, *2004*, 3792-3797; b) K. Y. Choi, Y. H. Matsuda, H. Nojiri, U. Kortz, F. Hussain and N. S. Dalal, *J. Phys. Conf. Ser.* **2006**, *51*, 95-98; c) K.-Y. Choi, N. S. Dalal, A. P. Reyes, P. L. Kuhns, Y. H. Matsuda, H. Nojiri, S. S. Mal and U. Kortz, *Phys. Rev. B* **2008**, *77*, 024406.
[43] a) U. Kortz, N. K. Al-Kassem, M. G. Savelieff, N. A. Al Kadi and M. Sadakane, *Inorg. Chem.* **2001**, *40*, 4742-4749; b) P. Mialane, J. Marrot, E. Rivière, J. Nebout and G. Hervé, *Inorg. Chem.* **2001**, *40*, 44-48; c) F. Chai, Y. Chen, Z. Yang, L. Su and Y. Sun, *J. Mol. Struct.* **2013**, *1051*, 101-106.

[44] K.-Y. Choi, N. S. Dalal, A. P. Reyes, P. L. Kuhns, Y. H. Matsuda, H. Nojiri, S. S. Mal and U. Kortz, *Phys. Rev. B* **2008**, *77*, 24406-24406.
[45] O. Oms, S. Yang, W. Salomon, J. Marrot, A. Dolbecq, E. Rivière, A. Bonnefont, L. Ruhlmann and P. Mialane, *Inorg. Chem.* **2016**, *55*, 1551-1561.
[46] L. David, C. Crăciun, V. Chis and R. Tetean, *Solid State Commun.* **2002**, *121*, 675-678.
[47] K. D. von Allmen, H. Grundmann, A. Linden and G. R. Patzke, *Inorg. Chem.* **2017**, *56*, 327-335.
[48] D. Rusu, A. R. Tomsa, G. L. Turdean, I. Cojocaru, O. Baban and M. Rusu, *Rev. Roum. Chim.* **2012**, *57*, 327-336.
[49] T. Yamase, B. Botar, E. Ishikawa and K. Fukaya, *Chem. Lett.* **2001**, *30*, 56-57.
[50] T. Yamase, E. Ishikawa, K. Fukaya, H. Nojiri, T. Taniguchi and T. Atake, *Inorg. Chem.* **2004**, *43*, 8150-8157.
[51] Y. Kohama, H. Kawaji, T. Atake, K. Fukaya and T. Yamase, *J. Solid State Chem.* **2009**, *182*, 1468-1472.
[52] X.-M. Liu, C.-R. Wang, B. Liu, G.-L. Xue, H.-M. Hu, J.-W. Wang and F. Fu, *Chin. J. Chem* . **2005**, *23*, 1412-1416.
[53] L. Wu, B. Liu, X. Dong, C. Yu, Y. Yan, H. Hu and G. Xue, *Inorg. Chem. Commun.* **2015**, *56*, 13-16.
[54] J.-m. Liu, L. Wang, K. Yu, Z.-h. Su, C.-x. Wang, C.-m. Wang and B.-b. Zhou, *New J. Chem.* **2015**, *39*, 1139-1147.
[55] a) R.-R. Cui, H.-L. Wang, X.-Y. Yang, S.-H. Ren, H.-M. Hu, F. Fu, J.-W. Wang and G.-L. Xue, *Chin. J. Chem* . **2007**, *25*, 176-181; b) L. Han, P.-P. Zhang, H.-S. Liu, H.-J. Pang, Y. Chen and J. Peng, *J. Cluster Sci.* **2010**, *21*, 81-91.
[56] D.-F. Chai, Z. Ma, H. Yan, Y. Qiu, H. Liu, H.-D. Guo and G.-G. Gao, *RSC Adv.* **2015**, *5*, 78771-78779.
[57] H. Liu, C. Qin, Y.-G. Wei, L. Xu, G.-G. Gao, F.-Y. Li and X.-S. Qu, *Inorg. Chem.* **2008**, *47*, 4166-4172.
[58] M. Sun, T. Wang, F. Li, Z. Sun and L. Xu, *New J. Chem.* **2018**, *42*, 7480-7484.
[59] H. Liu, Y. Liu, H. Liu, C. Shi, F. Liu and H. Liu, *Inorg. Chem. Commun.* **2009**, *12*, 1-3.
[60] B. Chen, W. Chen, W. Liu, Y. Li, X. Wang and E. Wang, *J. Coord. Chem.* **2011**, *64*, 71-81.
[61] H. Liu, L. Xu, G. Gao, F. Li and N. Jiang, *J. Mol. Struct.* **2008**, *878*, 124-130.
[62] Q. Wu, H. Ju, J. Tao, Z. Chen, J. Li, F. Wang, Q. Cai, L. Sun and X. Pan, *J. Cluster Sci.* **2015**, *26*, 1811-1820.
[63] Y. Liu, J. Cao, Y. Wang, Y. Li, J. Zhao, L. Chen, P. Ma and J. Niu, *J. Solid State Chem.* **2014**, *209*, 113-119.
[64] P. Ma, Y. Zhang and J. Li, *J. Coord. Chem.* **2014**, *67*, 2238-2248.
[65] U. Kortz, S. Nellutla, A. C. Stowe, N. S. Dalal, J. van Tol and B. S. Bassil, *Inorg. Chem.* **2004**, *43*, 144-154.
[66] R. Gupta, I. Khan, F. Hussain, A. M. Bossoh, I. M. Mbomekallé, P. de Oliveira, M. Sadakane, C. Kato, K. Ichihashi, K. Inoue and S. Nishihara, *Inorg. Chem.* **2017**, *56*, 8759-8767.
[67] H. Zhao, L. Tao, F. Zhang, Y. Zhang, Y. Liu, H. Xu, G. Diao and L. Ni, *Chem. Commun.* **2019**, *55*, 1096-1099.
[68] J. Hua, X. Ma, P. Ma, J. Wang and J. Niu, *J. Cluster Sci.* **2013**, *24*, 689-700.
[69] T. Yamase, K. Fukaya, H. Nojiri and Y. Ohshima, *Inorg. Chem.* **2006**, *45*, 7698-7704.
[70] T. Yamase, H. Ishikawa, H. Abe, K. Fukaya, H. Nojiri and H. Takeuchi, *Inorg. Chem.* **2012**, *51*, 4606-4619.
[71] Y. Oshima, H. Nojiri, K. Fukaya and T. Yamase, *J. Phys. Conf. Ser.* **2006**, *51*, 195-198.
[72] N. Zamstein, A. Tarantul and B. Tsukerblat, *Inorg. Chem.* **2007**, *46*, 8851-8858.
[73] Z. Zhao, B. Zhou, S. Zheng, Z. Su and C. Wang, *Inorg. Chim. Acta* **2009**, *362*, 5038-5042.
[74] J. Liu, J. Luo, Q. Han, J. Cao, L. Chen, Y. Song and J. Zhao, *J. Mater. Chem. C* **2017**, *5*, 2043-2055.
[75] A. Merca, A. Müller, J. van Slageren, M. Läge and B. Krebs, *J. Cluster Sci.* **2007**, *18*, 711-719.
[76] A. Merca, J. Schnack, J. van Slageren, T. Glaser, H. Bögge, V. Hoeke, M. Läge, A. Müller and B. Krebs, *J. Cluster Sci.* **2013**, *24*, 979-988.
[77] K.-Y. Wang, B. S. Bassil, X. Xing, B. Keita, J. K. Bindra, K. Diefenbach, N. S. Dalal and U. Kortz, *Eur. J. Inorg. Chem.* **2016**, *2016*, 5519-5529.
[78] K.-Y. Wang, Z. Lin, B. S. Bassil, X. Xing, A. Haider, B. Keita, G. Zhang, C. Silvestru and U. Kortz, *Inorg. Chem.* **2015**, *54*, 10530-10532.

[79] L. Chen, M. Jin, R. Zheng, Y. Liu and J. Zhao, *Inorg. Chem. Commun.* **2019**, *105*, 63-68.
[80] A. Dolbecq, J.-D. Compain, P. Mialane, J. Marrot, E. Rivière and F. Sécheresse, *Inorg. Chem.* **2008**, *47*, 3371-3378.
[81] D. Rusu, C. Roşu, C. Crăciun, L. David, M. Rusu and G. Marcu, *J. Mol. Struct.* **2001**, *563-564*, 427-433.
[82] M. Sun, F. Li, L. Yu, Y. Wang and L. Xu, *Dalton Trans.* **2016**, *45*, 2417-2421.
[83] a) U. Kortz, M. G. Savelieff, B. S. Bassil, B. Keita and L. Nadjo, *Inorg. Chem.* **2002**, *41*, 783-789; b) M. Carraro, B. S. Bassil, A. Sorarù, S. Berardi, A. Suchopar, U. Kortz and M. Bonchio, *Chem. Commun.* **2013**, *49*, 7914-7916.
[84] A. Sartorel, M. Carraro, G. Scorrano, B. S. Bassil, M. H. Dickman, B. Keita, L. Nadjo, U. Kortz and M. Bonchio, *Chem. Eur. J.* **2009**, *15*, 7854-7858.
[85] M. Prinz, A. F. Takács, J. Schnack, I. Balasz, E. Burzo, U. Kortz, K. Kuepper and M. Neumann, *J. Appl. Phys.* **2006**, *99*, 08J505-508J505.
[86] J. Jia, Y. Zhang, P. Zhang, P. Ma, D. Zhang, J. Wang and J. Niu, *RSC Adv.* **2016**, *6*, 108335-108342.
[87] J.-P. Wang, P.-T. Ma, J. Li, H.-Y. Niu and J.-Y. Niu, *Chem. Asian J.* **2008**, *3*, 822-833.
[88] L. Zhang, Y. Zhang, Z. Hao and F. Luo, *Z. Anorg. Allg. Chem.* **2010**, *636*, 1991-1997.
[89] L.-H. Bi, G.-F. Hou, Y.-Y. Bao, B. Li, L.-X. Wu, Z.-M. Gao, T. McCormac, S. S. Mal, M. H. Dickman and U. Kortz, *Eur. J. Inorg. Chem.* **2009**, *2009*, 5259-5266.
[90] C. Lu, Y. Chen, H. Li, L. Chen, C. Zhai and J. Zhao, *Inorg. Chem. Commun.* **2018**, *91*, 85-90.
[91] B. Artetxe, S. Reinoso, L. San Felices, P. Vitoria, A. Pache, J. Martín-Caballero and J. M. Gutiérrez-Zorrilla, *Inorg. Chem.* **2015**, *54*, 241-252.
[92] B. Artetxe, S. Reinoso, L. San Felices, L. Lezama, A. Pache, C. Vicent and J. M. Gutiérrez-Zorrilla, *Inorg. Chem.* **2015**, *54*, 409-411.
[93] J.-Q. Niu, Q. Zhao, X. Xin, Y.-Q. Zhang, N. Hu, Y.-Y. Ma and Z.-G. Han, *J. Coord. Chem.* **2020**, 1-11.
[94] H.-D. Wang, X.-F. Wang, F. Su, J.-S. Li, L.-C. Zhang, X.-J. Sang and Z.-M. Zhu, *Dalton Trans.* **2019**, *48*, 2977-2987.
[95] V. Das, R. Kaushik and F. Hussain, *Coord. Chem. Rev.* **2020**, *413*, 213271-213271.
[96] Y. Chen, L. Sun, S. Chang, L. Chen and J. Zhao, *Inorg. Chem.* **2018**, *57*, 15079-15092.
[97] J.-W. Zhao, J. Cao, Y.-Z. Li, J. Zhang and L.-J. Chen, *Cryst. Growth Des.* **2014**, *14*, 6217-6229.
[98] A. Kondinski, A. Menon, D. Nurkowski, F. Farazi, S. Mosbach, J. Akroyd and M. Kraft, *J. Am. Chem. Soc.* **2022,** doi.org/10.1021/jacs.2c03402.
[99] a) A. Kondinski and M. Ghorbani-Asl, *Nanoscale Adv.* **2021**, *3*, 5663-5675; b) A. Kondinski in *Computational modelling of isomeric polyoxometalates*, *Vol. 16* The Royal Society of Chemistry, **2021**, pp. 39-71.